NASA TECHNICAL NOTE

NASA TN D-4831

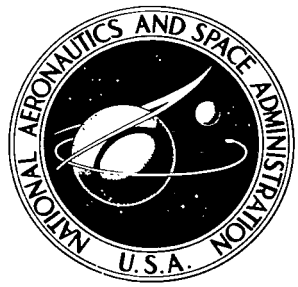

COMPUTER EXPERIMENTS ON THE MICROSCOPIC BEHAVIOR OF ONE-DIMENSIONAL PLASMAS

by Richard H. Weinstein and Belinda H. Adams

Langley Research Center
Langley Station, Hampton, Va.

NATIONAL AERONAUTICS AND SPACE ADMINISTRATION • WASHINGTON, D. C. • NOVEMBER 1968

COMPUTER EXPERIMENTS ON THE MICROSCOPIC BEHAVIOR OF ONE-DIMENSIONAL PLASMAS

By Richard H. Weinstein and Belinda H. Adams

Langley Research Center
Langley Station, Hampton, Va.

NATIONAL AERONAUTICS AND SPACE ADMINISTRATION

For sale by the Clearinghouse for Federal Scientific and Technical Information
Springfield, Virginia 22151 – CFSTI price $3.00

COMPUTER EXPERIMENTS ON THE MICROSCOPIC BEHAVIOR OF ONE-DIMENSIONAL PLASMAS*

By Richard H. Weinstein and Belinda H. Adams
Langley Research Center

SUMMARY

The detailed motions of a system of 1000 particles simulating a one-dimensional electrostatic plasma have been followed by using the IBM 7040/7094 Direct Coupled System at the Langley Research Center. The particle interactions are collective and, as the calculation proceeds stepwise through time, the position-velocity histories of all the particles completely specify the successive states of the system. These data constitute an "experiment," upon which measurements can be made. The velocity distribution function, the Fourier harmonics of the potential energy, the spatial correlations of the electric field, and the drag and velocity diffusion of "test particles" are measured for the Maxwellian and uniform velocity distributions. Comparison of the present work with both earlier experiments and the predictions of zeroeth and first-order plasma kinetic theory have yielded generally good agreement for all measurements in both equilibrium and non-equilibrium plasmas. The detailed behavior of the long wavelength harmonics of the potential energy is, however, unresolved for regions where the assumptions of the zeroeth-order theory are not satisfied.

INTRODUCTION

The large information-storage capacities and high calculating speeds of the digital computer have made possible a type of "computer experiment" which can provide rigidly controllable simulation of N-body interactions such as occur in plasmas. In contrast to Monte-Carlo techniques which are at best iterative, the computer experiments are dynamically self-consistent because they treat the simultaneous motion of all N particles due to the instantaneous, self-consistent Coulomb field of the charged particles. This method can be viewed as an experiment against which the predictions of theory may be checked.

---

*The information presented herein was offered as a thesis in partial fulfillment of the requirements for the degree of Master of Science in Physics, Virginia Polytechnic Institute, Blacksburg, Virginia, June 1967.

Although some three-dimensional problems (ref. 1) have been studied, the number of particles treated is generally modest, both because of the large amount of information storage required for each particle and because of the complexity of the calculations in several dimensions (for example, solution of the self-consistent potential). The simplicity of one-dimensional models allows the use of large numbers of particles and thereby improves the statistical accuracy of the results. A one-dimensional model can be constructed by visualizing the particles as parallel sheets and allowing them to pass through (that is, cross) each other. Such models, used in the one-dimensional plasma diode experiments initiated by Hartree and Nicholson (1943, unpublished) and continued by Lomax (ref. 2), Birdsall and Bridges (refs. 3 and 4), and by Burger (ref. 5), can provide realistic dynamic simulation of a laboratory experiment and thereby serve as a guide to developing a theory. Conversely, the theoretically predicted two-stream instability was first observed "experimentally" by Buneman (ref. 6) in a computer experiment. Monte-Carlo calculations, such as those of Goldstein (ref. 7) solve only for the steady state of the diode, and self-consistency is approached iteratively. Quasi-one-dimensional models have been used for problems involving magnetic fields, such as the ion-cyclotron wave calculation of Hasegawa and Birdsall (ref. 8). A rather sophisticated one-dimensional model treated by Dawson (ref. 9) has included self-consistent electromagnetic radiation. Several two-dimensional experiments have been used as engineering tools; for example, Buneman and Kooyers (ref. 10) studied the ion engine neutralization problem, and Yu, Kooyers, and Buneman (ref. 11) used a model of the magnetron which could, in principle, be used to design tubes. A complete summary of recent work in both computer experiments and simulation of plasmas by computer solution of the governing equations can be found in reference 12.

This work follows the approaches of Eldridge and Feix (refs. 13 and 14) and Dawson (refs. 15 and 16), who were concerned with checking predictions of the Vlasov-Landau theory, rather than simulating an experimental situation. An approximate computer program is used in which several particle crossings are allowed per time step of the calculations; this approach has made it practical to treat larger numbers of particles per Debye distance (nD), that is, more nearly collisionless (Vlasov) plasmas, and to follow the plasmas for long times. The accuracy of the calculation is checked both through conservation of energy and by its agreement with the Vlasov theory predictions checked in earlier experiments with exact models (refs. 13 to 16).

Studies of nonequilibrium plasmas are the principal extension of this work over that of references 13 to 16. Eldridge and Feix (ref. 14) predicted a stationary state or "metaequilibrium" in one dimension for any stable distribution function; this phenomenon was first observed by Dawson (ref. 16). The larger values of nD used in this report show the expected improvement in stationarity of the distribution function.

A brief review of the kinetic theory is provided as an introduction to the potential energy harmonic and spatial correlation theory. Measurements of the Fourier harmonics of the potential energy and the electric-field spatial correlation are repeated for a nonequilibrium plasma. The first-order kinetic theory is presented next, although the metaequilibrium, a first-order result, underlies even the Vlasov nonequilibrium studies. The drag and velocity diffusion of test particles are measured both to check the scaling predictions of the kinetic theory and its quantitative accuracy.

SYMBOLS

A	normalizing coefficient of one-particle distribution function
a	limiting velocity of square distribution
C	autocorrelation function
c	mode number of Fourier component
D	Debye distance
D_2, D_3	Debye distance analog for $f_2(v)$ and $f_3(v)$, respectively
E	electric field
$\overline{E}$	dimensionless electric field, $\frac{E}{4\pi\sigma}$
$\mathcal{F}$	N-particle distribution function
F	reduced many-particle distribution function
f	one-particle distribution function
g	graininess parameter, $\frac{1}{nD}$
Im( )	imaginary part of variable
k	wave number
L	length of system

l_ρ, l_∞	contours shown in figure 4
m	mass per unit area of sheet particles
m_e	mass per unit area of electron sheets
N	total number of particles
n	system particle density, N/L
P	pair distribution function
q	number of particles described by distribution function F_q
Re( )	real part of variable
r	exponential power index of one-particle distribution function
s	Laplace transform variable, complex frequency
T	dimensionless time, $\omega_p t$
t	time
V	dimensionless velocity, $\frac{v}{v_T}$
v	velocity
v_T	thermal velocity or root-mean-square velocity
W	energy
x	position
y	dummy variable
α	acceleration

β normalization factor in one-particle distribution function given in dimensions of $\left(\frac{1}{v_T}\right)^r$

γ order of expansion parameter

ϵ plasma dielectric constant

η total energy growth rate

θ angle in complex plane

λ electric-field correlation length

μ charge-to-mass ratio of particles normalized to electron values, $\frac{\sigma_i}{m_i}\left(\frac{m_e}{\sigma}\right)$

ρ charge number density

σ absolute value of the charge per unit area of electron sheets

τ nondimensional relaxation time, $\frac{\omega_p t}{nD}$

ϕ Fourier-Laplace transform of one-particle distribution function

χ Fokker-Planck drag coefficient

ψ Fokker-Planck diffusion coefficient

$\Omega = \frac{\omega_p}{\omega_k}$

ω radian frequency

ω_p plasma frequency, $\frac{4\pi n\sigma^2}{m}$

Subscripts:

h,i,j indexing parameters

A bar over a symbol denotes a nondimensional value; an arrow over a symbol denotes a vector. Average values are denoted by $< >$. Primes denote perturbed quantities and an asterisk denotes a complex conjugate.

EXPERIMENTAL SYSTEM

Model and Equations of Motion

The plasma is simulated by following the motions of large, plane, parallel sheets confined to one-dimensional motions along an axis normal to the sheets. Equal numbers of positively and negatively charged sheets are used so that the total system is electrically neutral. The total number of sheets in the system is taken to be N and all sheets have the same mass density. Each sheet is acted on by the collective coulomb forces of all the other sheets. The electric field in the system is a step function; it is constant between sheets and changes by $\pm 4\pi\sigma$ in crossing a sheet, where σ is the charge per unit area of an electron sheet. A field configuration for a typical plasma having eight particles is shown in figure 1(a), where the circles represent the value of the field at the position of the sheets.

The sheets, or "particles" as they will be called henceforth, are allowed to pass through each other (that is, cross). The system is considered to be periodic; thus, the motion of the particles is followed only between two imaginary boundaries at $x = 0$ and $x = L$. This condition is physically equivalent to representing an infinite plasma by a periodic structure of fundamental wavelength L, and thereby placing a maximum wavelength constraint on the Fourier representation of system quantities, such as density and potential energy. To describe an infinite plasma with this model successfully, it is required that $L/D \gg 1$, where D is the Debye distance, the characteristic scale length for a plasma. For computational purposes, the system may also be viewed as having its two ends ($x = 0$ and $x = L$) tied together.

Particles leaving this interval are accounted for by cumulative charge sums kept on the wall crossed where σ_0 is the charge at $x = 0$ and σ_{N+1} is the charge at $x = L$. When a particle crosses a boundary, its "twin" (a particle with the same charge and velocity vector) is injected at the opposite wall along with a compensating charge kept on the opposite wall. This condition is shown in figure 1(b), where particle 8 has crossed the boundary at $x = L$ and has been reinserted at $x = \Delta$. The field change across σ_8 is $-4\pi\sigma$; thus, $+4\pi\sigma$ and $-4\pi\sigma$ are added, respectively, to σ_0 and σ_{N+1}, and the twin particle 8' appears near $x = 0$. This manipulation of boundary charges maintains the self-consistency of the field in the plasma regardless of events at the boundary. Thus, for example, the field seen by particle 7 remains at $+2\pi\sigma$; without the addition of σ_0 and σ_{N+1}, this field would have been $-2\pi\sigma$ after the crossing, and the conservation of electrostatic (that is, potential) energy in the system would have been destroyed.

Because of charge neutrality, the electric field has the same value at $x = 0$ and $x = L$, although it may be nonzero because of fluctuations of σ_0 and σ_{N+1}. At a given

time t, the force per unit area experienced by a representative sheet at position x_j is

$$m\ddot{x}_j = \sigma_j E(\ddot{x}_j, t) \tag{1}$$

where σ_j is the charge per unit area, $E(x_j,t)$ is the electric field, m is the mass per unit area, and $\ddot{x}_j$ is the acceleration of the jth sheet. The self-consistent field seen by the sheet is given by a sum over all the other sheets; that is

$$E(x_j,t) = 2\pi\left[\sum_{i=0}^{N+1} \sigma_i \operatorname{sgn}(x_i(t) - x_j(t))\right] \tag{2a}$$

where

$$\operatorname{sgn}(x) = \begin{cases} +1 & (x > 0) \\ 0 & (x = 0) \\ -1 & (x < 0) \end{cases}$$

The charge densities σ_i are henceforth referred to as charges. Because of charge neutrality in the interval 0 to L, $E(x_j,t)$ may be more simply calculated as

$$E(x_j,t) = 4\pi \sum_{x_i<x_j} \sigma_i + 2\pi\sigma_j \tag{2b}$$

where the summation extends over all i such that $x_i < x_j$.

The field seen by a particle changes, in general, when it crosses a neighbor, as is shown in figure 1(c). Here, particles 2 and 3 have crossed, and the field seen by particle 2 has changed from $-2\pi\sigma$ to $-6\pi\sigma$. To calculate the exact evolution of the system, it is necessary to calculate the time at which this crossing occurs, to advance the particles concerned to the crossing point, and then to recalculate the electric field to be used for the next step of the motion. Because the number of crossings that must be considered increases both with the total number of particles and nD, the range of problems feasible with such an exact program is somewhat limited because of the long calculation times necessary. Such an exact program was used by Eldridge and Feix (refs. 13 and 14).

This paper uses an approximate program based on the integral of equation (1) over a small fixed time step Δt; the initial field $E(x_j,t)$ is taken as the forcing term for the motion over the time step and the field is recalculated only at the end of the time step. If the size of the time step is small compared with the inverse plasma frequency, which serves as a fundamental scaling time for the plasma, few crossings leading to only small errors in the particle motion will have occurred. These crossings destroy the strict conservation of energy possible with the exact program within computer truncation error, and the extent of departure from strict conservation provides a criterion of acceptability for the approximate program. The errors in particle motion are due to the fact that crossings make the electric field a function of time during the motion. The electric field

$E(x_j,t)$ will, in fact be discontinuous, but if the particle motion is to be recalculated only at the end of each time step, one may smooth the field over a time Δt and obtain correction terms from a Taylor series expansion; for example, with $\Delta t = t_2 - t_1$,

$$E(x_j,t_2) = E(x_j,t_1) + \dot{E}(x_j,t_1)\Delta t + \frac{1}{2}\ddot{E}(x_j,t_1)\Delta t^2 + \ldots$$

These time derivatives may be approximated by their backward difference equivalents, for example,

$$\dot{E}(x_j,t_1) = \frac{E(x_j,t_1) - E(x_j,t_1 - \Delta t)}{\Delta t} \tag{3}$$

Integration of equation (1) from $t = 0$ to $t = \Delta t$ gives for the position and velocity of the jth particle,

$$x_j(t_1 + \Delta t) = x_j(t_1) + v_j(t_1)\Delta t + \frac{\sigma_j}{m}\left[\frac{1}{2}E(x_j,t_1)\Delta t^2 + \frac{1}{6}\dot{E}(x_j,t_1)\Delta t^3 + \ldots\right] \tag{4a}$$

$$v_j(t_1 + \Delta t) = v_j(t_1) + \frac{\sigma_j}{m}\left[E(x_j,t_1)\Delta t + \frac{1}{2}\dot{E}(x_j,t_1)\Delta t^2 + \frac{1}{6}\ddot{E}(x_j,t_1)\Delta t^3 + \ldots\right] \tag{4b}$$

The time increment Δt is taken to be small and terms of order Δt^3 and higher are neglected; as a result, the equations of motion can be truncated after the $(\Delta t)^2$ term. To this order, the time dependence of $E(x_j,t)$ gives rise to the $(\Delta t)^2$ term in the velocity equation, which would not appear in a constant-force situation; the strong effect of this term on the conservation of energy is shown.

Equations (4a) and (4b) can be simplified by normalization in terms of characteristic parameters of the plasma, namely, D the Debye distance, v_T the thermal velocity (the root mean square velocity for an equilibrium plasma), and $\omega_p \equiv \sqrt{\frac{4\pi n\sigma^2}{m_e}}$ the plasma frequency. These quantities are interrelated by the definition $D = \frac{v_T}{\omega_p}$. Also of interest are the following dimensionless quantities:

$$V_j = \frac{v_j}{v_T}$$

$$\Delta T = \Delta t\omega_p$$

With the normalizations,

$$\bar{E}(x_j,t) = \frac{E(x_j,t)}{4\pi\sigma}$$

and

$$\bar{\sigma}_j = \frac{\sigma_j}{\sigma}$$

equations (4a) and (4b) become

$$x_j(T_1 + \Delta T) = x_j(T_1) + V_j(T_1) D\,\Delta T + \frac{1}{2}\frac{\overline{\sigma_j}}{n}\overline{E}(x_j, T_1)\Delta T^2 \tag{5a}$$

$$V_j(T_1 + \Delta T) = V_j(T_1) + \frac{\overline{\sigma_j}}{nD}\left[\overline{E}(x_j, T_1)\Delta T + \frac{1}{2}\overline{\dot{E}}(x_j, T_1)\Delta T^2\right] \tag{5b}$$

The position x_j is not normalized to the Debye distance D for reasons of convenience and in the computer program the density $n = \frac{N}{L}$ is taken to be unity.

Initial Condition

The initial state of the plasma is one of uniform particle density; the particles are equidistant from one another in the interval $x = 0$ to $x = L$ and electrons and ions alternate. This configuration is the minimum potential energy state of the uniform system and was chosen because of its computational convenience. Individual particle velocities are initially chosen from a pseudo-random number generator. Both velocity distributions used in the experiments described here are of the form $f(v) = A \exp(-\beta v^r)$, where r is a positive number. The quantities A and β are independent of v but are determined by the normalization of $f(v)$ and the second moment of $f(v)$, respectively. The values $r = 2$ and $r = \infty$ give the Maxwellian $[f_1(v)]$ and uniform $[f_3(v)]$ distributions, respectively. These velocity distributions are shown in figure 2, along with $f_2(v)$, the Druyvesteyn distribution ($r = 4$) which proves to be an interesting intermediate step in the transition of the uniform distribution $f_3(v)$ to equilibrium.

All distributions are normalized to have the same total kinetic energy for a given value of D. This requirement dictates the sharp cutoff of the uniform distribution yielding $f_3(v)$ which will henceforth be referred to as the "square" distribution. The Maxwellian distribution has an effective cutoff less than $2.5v_T$ because of the finite number of particles considered and the exponentially decreasing form of the distribution function.

It should be noted that for each type of velocity distribution (that is, Maxwellian or square), the same set of pseudo-random numbers is used for all values of nD. Changing nD is, however, sufficient to give different time histories to each plasma (Δt being held constant) because, for example, a particle traveling with the thermal velocity through a plasma of density n crosses nD particles per ΔT. Thus the electric field seen by each particle is, in general, different even after the first time step, because the different numbers of crossings for each value of nD give different charge configurations. The

scaling of first-order plasma kinetics with nD is not, therefore, a trivial result of scaling the equations of motion, but is shown to be a prediction of plasma kinetic theory.

Computational Information

The computer time necessary to advance all particles through one cycle (that is, to update the system from time T to time $T + \Delta T$) depends on both the system size and the plasma parameters. For the range of conditions studied here, this time is empirically given for the IBM 7040/7094 Directly Coupled System in seconds as

$$T_{cycle} = 5N \times 10^{-4} + 0.89NnD\,\Delta T \times 10^{-4}$$

The first term in this equation represents the time necessary to calculate the new positions and velocities for all N particles from stored or calculated quantities. The second term is due to calculation of the electric field. Because the field seen by a particle depends on the excess charge on either side of it, a table of identification numbers giving the order of particles is recomputed each time the particle positions are recalculated.

The time necessary to accomplish this computation obviously depends on the size of the time step (longer times yield more crossings), and the necessity of scaling with nD can be seen from the fact that a particle traveling at the thermal velocity crosses (on the average) nD particles in a time ω_p^{-1}. Typically, for a plasma of 1000 particles with $nD = 40$ and $\Delta T = 0.1$, the cycle time is ≈ 0.83 second. This time represents considerable improvement over an exact program, which has a speed comparable to the approximate program for $nD = 10$, but the time unfortunately grows as ND rather than as nD. As the calculations proceed stepwise through time, the position and velocity of each particle along with the total kinetic and potential energy are stored on magnetic tape at each cycle or desired multiple thereof. These data are used as inputs for the measurements described subsequently. Some of the techniques used in the plasma generation and measurement programs are discussed in the appendix.

Conservation of Energy

The energy calculation shows the effect of including $\dot{E}$ in equation (5b). Whereas the conservation of energy for the exact program is precise (within the limits of computer precision), the total energy grows slowly as a function of time with the approximate program. The rate of total energy increase, scaled to the initial energy and the plasma frequency, is taken as

$$\eta = \frac{(\Delta W_{tot})\omega_p}{(W_{tot})_0}$$

where $(W_{tot})_0$ is the total initial energy, ΔW_{tot} is the difference between final and initial energy.

Figure 3 shows this growth rate as a function of the size of the time step for a range of values of nD. Note that different values of nD correspond to plasmas at different temperatures, for $D^2 = \left(\frac{v_T}{\omega_p}\right)^2 \propto$ (Kinetic energy). If the motion in equation (5b) is calculated without $\dot{E}$, the empirically determined form of the energy growth rate is found to be

$$\eta = \frac{\Delta T}{2(nD - 1)}$$

This expression is valid over the range of ΔT shown in figure 3. Comparison between curves with and without $\dot{E}$ for corresponding values of nD shows that one can increase the size of ΔT by about a factor of four for a specified accuracy; this increase in ΔT proportionately decreases the time needed to advance the system one time step. This decrease is the justification for using an approximate program for Vlasov plasmas. Although the number of crossings and, therefore, the deviations from strict accuracy increase with nD, the smoothing of fluctuations in the fluid limit aids the gross physical consistency.

ZEROETH-ORDER THEORY AND MEASUREMENTS

The Plasma Kinetic Theory

Experiments using the plasma model described have been compared with predictions of both zeroeth and first-order kinetic theory derived from the Bogoliubov-Born-Green-Kirkwood-Yvonne (BBGKY) heirarchy (ref. 17) outlined briefly below for a one-dimensional system (ref. 18). The starting point is the Liouville theorem, which describes the motion of an ensemble of identical systems in 2N-dimensional phase space (that is, x,v space), where N is the number of particles in each system. The state of each system in the ensemble is denoted by one point in phase space. If

$$\mathcal{F}\left(x_1, v_1, \ldots, x_N, v_N, t\right) \prod_{i=1}^{N} dx_i\, dv_i$$

represents the probability of finding a system at a particular point in phase space at a time t, with particle 1 between x_1 and $x_1 + dx_1$, and so forth, and is normalized so that

$$\int_{-\infty}^{\infty} \cdots \int_{-\infty}^{\infty} \mathcal{F} \prod_{i=1}^{N} dx_i\, dv_i = 1$$

then the Liouville theorem for the system states that

$$\left[\frac{\partial}{\partial t} + \sum_{i=1}^{N}\left(v_i \frac{\partial}{\partial x_i} + \alpha_i \frac{\partial}{\partial v_i}\right)\right]\mathcal{F} = 0 \tag{6}$$

where α_i is the acceleration experienced by the ith particle.

If one defines the reduced q-particle distribution function as

$$F_q = L^q \int_{-\infty}^{\infty} \cdots \int_{-\infty}^{\infty} \mathcal{F} \prod_{i=q+1}^{N} dx_i\, dv_i \tag{7}$$

where L is the length of the system, then multiplication of equation (6) by

$$L^q \prod_{i=q+1}^{N} dx_i\, dv_i$$

and integration over N - q coordinates yields a linked set of equations giving F_q in terms of F_{q+1}; that is, use of the indistinguishability of the N - q particles and neglect of surface integrals at the phase-space boundary yields

$$\left(\frac{\partial}{\partial t} + \sum_{i=1}^{q} v_i \frac{\partial}{\partial x_i} + \sum_{i,j=1}^{q} \alpha_{i,j} \frac{\partial}{\partial v_i}\right) F_q = - \sum_{i=1}^{q} \frac{N - q}{L} \int_{-\infty}^{\infty} dx_{q+1}\, dv_{q+1} \alpha_{i,q+1} \frac{\partial F_{q+1}}{\partial v_i} \tag{8}$$

In equation (8), $\alpha_{i,j} = \left(\frac{\sigma}{m}\right)_i E_{ij} = \left(\frac{\sigma}{m}\right)_i 2\pi\sigma_j \operatorname{sgn}(x_i - x_j)$ is the acceleration of the ith particle due to its interaction with the jth particle; that is, external fields are taken to be zero. Dependence of F_q on F_{q+1} arises from a sum over the two-particle interaction potential $\alpha_{i,q+1}$ so that in principle, all the higher order functions must be known in order to determine the kinetic equation for any given function F_q. The system must be large enough ($N \to \infty$, $L \to \infty$) to insure that the graininess expansion parameter (to be introduced next) is still large compared with perturbations n'/n where $n = \frac{N}{L}$ = Constant is the equilibrium density.

The graininess expansion is introduced by proceeding to a fluid limit description of the plasma. For a large system, one conceptually splits each particle so that the electronic charge and mass densities (σ and m) become very small, and simultaneously defines the limits that σ/m is constant and that nm and $n\sigma$ remain finite. Although this fluid limit is a purely mathematical construction, a real plasma exhibits the same type of fluid properties because long-range coulomb forces result in collective behavior. Equation (8) may be made dimensionless by introducing the plasma frequency, thermal velocity, electron charge, and charge-mass ratio

$$\mu_i = \frac{\sigma_i}{m_i}\left(\frac{m_e}{\sigma}\right)$$

where m_e and σ refer to the absolute values of electron quantities. Electric fields are normalized in terms of the sheet charge density, that is, E is normalized as $\overline{E} = \frac{E}{4\pi\sigma}$. This normalization gives rise to the so-called graininess parameter

$$g = \left(\frac{4\pi\sigma^2}{nmv_T^2}\right)^{1/2} = \frac{\omega_p}{nv_T} = \frac{1}{nD}$$

which, for large nD, may be used as an expansion parameter for the linked equations. If the q-particle distribution function F_q is expanded in orders of g, that is,

$$F_q = F_q^{\,0} + gF_q^{\,1} + g^2F_q^{\,2} + \ldots + g^\gamma F_q^{\,\gamma} + \ldots \tag{9}$$

Then substitution into equation (8) yields, after separation by powers of g, dimensionless kinetic equations to any desired order γ; that is,

$$\frac{\partial F_q^{(\gamma)}}{\partial t} + \sum_{i=1}^{q}\left[v_i \frac{\partial F_q^{(\gamma)}}{\partial x_i} + \frac{1}{2}\mu_i \int_{-\infty}^{\infty} \overline{\sigma_{q+1}}\, dx_{q+1}\, dv_{q+1}\, \mathrm{sgn}(x_i - x_{q+1}) \frac{\partial F_{q+1}^{(\gamma)}}{\partial v_i}\right]$$

$$= -\frac{1}{2}\sum_{i=1}^{q} \mu_i \sum_{j=1}^{q} \overline{\sigma_j}\, \mathrm{sgn}(x_i - x_j) \frac{\partial F_q^{(\gamma-1)}}{\partial v_i} \tag{10}$$

Complications in equation (10) arise because $F_q^{(\gamma)}$ is given both in terms of $F_q^{(\gamma-1)}$ and $F_{q+1}^{(\gamma)}$. The ordering in powers of g is equivalent to introducing a hierarchy of time scales in which the λth-order kinetic equation describes $\partial F_q / \partial \tau_\gamma$ where $\tau_\gamma = \frac{(nD)^\gamma}{\omega_p}$ is the γth-order time scale. As a final step, some relation between F_q and F_{q+1} must be specified. The Mayer cluster expansion (ref. 17) is the usual choice and gives the following form:

$$F_1^{(1)} = F_1^{(0)}(1)$$

$$F_2(1,2) = F_1^{(0)}(1)F_1^{(0)}(2) + P(1,2)$$

$$F_3(1,2,3) = F_1^{(0)}(1)F_1^{(0)}(2)F_1^{(0)}(3) + F_1^{(0)}(1)P(2,3) + F_1^{(0)}(2)P(1,3) + F_1^{(0)}(3)P(1,2) + T(1,2,3)$$

In this expansion, $P(1,2) = gF_2^{(1)}(1,2)$ is the pair correlation function and $T(1,2,3) = g^2F_3^{\,2}(1,2,3)$ is the triplet correlation function. The chain of equations may then be formally broken by neglecting small quantities – in this case, any term of order g^2 or higher.

To zeroeth order, one obtains the dimensionless Vlasov equation (ref. 18),

$$\left[\frac{\partial}{\partial t} + v_1 \frac{\partial}{\partial x_1} + \mu_1 \overline{E}^{(0)} \frac{\partial}{\partial v_1}\right] f(1) = 0 \tag{11}$$

where $f(1) = F_1^{(0)}(1)$ is the usual one-particle distribution function and $E^{(0)}$ is the self-consistent field determined by Poisson's equation; that is,

$\overline{E}^{(0)} = \frac{1}{2}\int_{-\infty}^{\infty} dx_2\, dv_2 \overline{\sigma_2}\, \mathrm{sgn}(x_1 - x_2) f(2)$. If a homogeneous system is considered, the first-order equation for the total one-particle distribution function is, from equation (10) with $q = 1$, $\gamma = 1$,

$$\frac{\partial f(1)}{\partial t} = \frac{\mu_1}{2} \frac{\partial}{\partial v_1} \int_{-\infty}^{\infty}\int_{-\infty}^{\infty} \overline{\sigma_2}\, dx_2\, dv_2\, \mathrm{sgn}(x_1 - x_2) P(1,2) \tag{12}$$

and $P(1,2)$, in turn, satisfies the first-order equation for $q = 2$, $\gamma = 1$:

$$\left(\frac{\partial}{\partial t} + v_1 \frac{\partial}{\partial x_1} + v_2 \frac{\partial}{\partial x_2}\right) P(1,2) + \frac{\mu_1}{2} \overline{\sigma_3} \int_{-\infty}^{\infty} dx_3 \int_{-\infty}^{\infty} dv_3 \left[\mathrm{sgn}(x_1 - x_3) P(1,3) \frac{\partial f(1)}{\partial v_1}\right]$$

$$+ \frac{\mu_2}{2} \overline{\sigma_3} \int_{-\infty}^{\infty} dx_3 \int_{-\infty}^{\infty} dv_3 \left[\mathrm{sgn}(x_2 - x_3) P(2,3) \frac{\partial f(2)}{\partial v_2}\right] = \frac{g}{2} \mathrm{sgn}(x_1 - x_2) \left[\mu_1 \overline{\sigma_2} f(2) \frac{\partial f(1)}{\partial v_1}\right.$$

$$\left. - \mu_2 \overline{\sigma_1} f(1) \frac{\partial f(2)}{\partial v_2}\right] \tag{13}$$

Subscripts and numbers in parentheses in equation (12) correspond to specific particles. The Vlasov equation (eq. (11)) provides the basis for interpreting the potential-energy spectrum and electric-field correlation measurements; the first-order kinetic equations (eqs. (12) and (13)) provide the relaxation theory.

Vlasov Theory

Solution of the Vlasov equation for a homogeneous one-dimensional system (refs. 19 and 20) is conveniently handled by using the symmetric Fourier-Laplace transform of the one-particle distribution function; that is

$$\phi(k,v,s) = \frac{1}{2\pi}\int_{-\infty}^{\infty} dx \int_{0}^{\infty} dt\, f(x,v,t) \exp(ikx) \exp(-st)$$

and similar transforms for other functions of x and t. For a system composed of point particles, the δ-function density in position space is changed by a Fourier transform

into a sum of continuous functions in k-space. The Laplace transform on time introduces initial conditions into equation (11); that is, if $\phi(k,v,s)$ is the Laplace transform of a function $f(x,v,t)$, then

$$\int_{-\infty}^{\infty} dx \exp(ikx) \int_{0}^{\infty} dt \frac{\partial f(x,v,t)}{\partial t} \exp(-st) = s\phi(k,v,s) - f(k,v,t=0)$$

If one takes

$$\int_{-\infty}^{\infty} dx \int_{-\infty}^{\infty} dv\, f(x,v,t) = 1$$

one can consider a perturbed one-particle distribution function of the form

$$\Phi = \phi^0(v) + \phi'(k,v,s) \tag{14}$$

where ϕ^0 is the homogeneous velocity distribution function and $\phi'(k,v,s)$ is a small perturbation. The integral of this perturbation over phase space must be zero. The perturbed distribution function $\phi'(k,v,s)$ gives rise to a perturbed electric field $E'(k,s)$ so that substitution of equation (14) into the dimensional Vlasov equation and linearization $\left(\text{that is, neglect of the second-order of } E' \frac{\partial f'}{\partial v} \text{ term}\right)$ gives for ions (+) and electrons (-), respectively,

$$\phi'_{\pm}(k,v,s) = \frac{1}{s - ikv}\left[\phi'_{\pm}(k,v,t=0) - \left(\frac{\sigma}{m}\right)_{\pm} E'(k,s)\frac{\partial f^0_{\pm}(v)}{\partial v}\right] \tag{15}$$

It is to be noted that $f^0(v) = \phi^0(v)$ and is the unperturbed distribution function which is a function only of velocity. Here the externally applied field is still assumed to be zero and the perturbed linearized field is given by the Fourier-Laplace transform of Poisson's equation

$$\int_{-\infty}^{\infty} dx \int_{-\infty}^{\infty} dt \exp(ikx - st)\frac{\partial E'(x,t)}{\partial x} = 4\pi\sigma n \int_{-\infty}^{\infty} dx \int_{-\infty}^{\infty} dt \exp(ikx - st) \int_{-\infty}^{\infty}\left(f'_- - f'_+\right)dv$$

or

$$-ikE'(k,s) = 4\pi\sigma n \int_{-\infty}^{\infty} dv\left[\phi'_-(k,v,s) - \phi'_+(k,v,s)\right] = 4\pi\rho(k,s) \tag{16}$$

where σ is the charge density of an electron sheet, and all fields are taken to be zero at infinity.

If both species have the same mass density and distribution function, then combination of the electron and ion equations through the use of Poisson's equation gives for $\rho(k,s)$ the net charge density,

$$\rho(k,s) = \frac{\sigma}{\epsilon(k,s)} \int_{-\infty}^{\infty} \frac{\phi'(k,v,t=0)}{s - ikv}\, dv \tag{17}$$

where

$$\epsilon(k,s) = 1 + \frac{i\omega_p^2}{k^2} \int_{-\infty}^{\infty} \frac{\partial f^0/\partial v}{\frac{s}{k} - iv}\, dv \tag{18}$$

is the plasma dielectric function, which contains a complete description of the collective aspects of the plasma (refs. 19 and 20). The Laplace transform variable s is complex, and $\mathrm{Re}(s)$ represents growth or decay of oscillation amplitudes and $\mathrm{Im}(s)$ represents a wave propagation frequency ω. For $\mathrm{Re}(s) = 0$, $\epsilon(k,s) = 0$ gives a dispersion relation for the usual plasma oscillations; recovery of a small $\mathrm{Re}(s)$ gives the Landau damping (ref. 17).

For our purposes, it will be more convenient to work with frequency ω, rather than with the Laplace variable s. If $s = i\omega$, then the Fourier density function can be shown to be (refs. 21 and 22)

$$\left\langle \left|\rho(k,\omega)\right|^2 \right\rangle = \frac{n\sigma^2}{|k|} \frac{f^0\left(\frac{\omega}{k}\right)}{\left|\epsilon(k,\omega)\right|^2} \tag{19}$$

where $f^0\left(\frac{\omega}{k}\right)$ is the value of the unperturbed one-particle distribution function at $v = \frac{\omega}{k}$ and ω is a real frequency. This relation is very general, as pointed out by Rostoker (ref. 21), and represents an extension of the Nyquist fluctuation dissipation theorem through the generalized dielectric function $\epsilon(k,\omega)$. As such, it relates the fluctuations to the correlations wherever a stationary distribution function can be defined (ref. 22).

It can be shown (ref. 21) that the Fourier transform of the spectral density function is the autocorrelation function $C(\lambda,\tau)$. If the symmetric Fourier transforms are defined as

$$E(x,t) = \frac{1}{2\pi} \int_{-\infty}^{\infty} dk \int_{-\infty}^{\infty} d\omega\, E(k,\omega) \exp\left[-i(kx + \omega t)\right]$$

$$E(x+\lambda,t+\tau) = \frac{1}{2\pi} \int_{-\infty}^{\infty} dk' \int_{-\infty}^{\infty} d\omega'\, E(k',\omega') \exp\left[-i(k'x + \omega' t)\right] \exp\left[-i(k'\lambda) + \omega'\tau)\right]$$

use of Poisson's equation (eq. (16)) gives for the autocorrelation function,

$$C(\lambda,\tau) = \langle E(x,t)\ E^*(x+\lambda,t+\tau)\rangle_{x,t} = \frac{1}{2\pi}\int_{-\infty}^{\infty} dk \int_{-\infty}^{\infty} d\omega \langle |E(k,\omega)|^2 \rangle e^{i(k\lambda+\omega\tau)}$$

$$= 8\pi \int_{-\infty}^{\infty} dk \int_{-\infty}^{\infty} d\omega \frac{\langle |\rho(k,\omega)|^2 \rangle}{k^2} e^{i(k\lambda+\omega\tau)} \quad (20a)$$

where the Fourier density functions are given by their ensemble averages.

For $\lambda = \tau = 0$, $\overline{C}(\lambda,\tau) = \dfrac{C(\lambda,\tau)}{8\pi m v_T^2} \times L$ is the potential energy of the system normalized to twice the kinetic energy; that is,

$$\overline{C}(0,0) = \frac{C(0,0) \times L}{8\pi m v_T^2} = \frac{L}{m v_T^2} \frac{\langle |E|^2 \rangle_{x,t}}{8\pi} = \frac{L}{4\pi D^2} \int_{-\infty}^{\infty} dk \int_{-\infty}^{\infty} d\omega \frac{\langle |\rho(k,\omega)|^2 \rangle}{n\sigma^2 k^2}$$

Thus,

$$\overline{C}(0,0) = \frac{L}{4\pi D^2} \int_{-\infty}^{\infty} dk \frac{\langle |\rho(k)|^2 \rangle}{n\sigma^2 k^2} = \int_{-\infty}^{\infty} dk\ W(k) \quad (20b)$$

In equation (20b) the integration on ω has been performed and the remaining integrand $W(k)$ gives the Fourier harmonics of the normalized potential energy. If $\lambda \neq 0$, one obtains $\overline{C}(\lambda,0)$ the normalized spatial correlation of the electric field, which is related to the Debye screening; that is,

$$\overline{C}(\lambda,0) = \frac{L}{8\pi m v_T^2} \langle E(x,t)\ E^*(x+\lambda,t)\rangle = \frac{L}{4\pi D^2} \int_{-\infty}^{\infty} dk \frac{\langle |\rho(k)|^2 \rangle}{n\sigma^2 k^2} e^{ik\lambda} \quad (20c)$$

The quantity $E(x)\ E^*(x+\lambda)$ can be directly measured in the plasma, whereas its analytic form can be determined by integration of equations (20b) and (20c) for a specific $f(v)$. The distribution function appears both explicitly in the $f^0\left(\frac{\omega}{k}\right)$ factor and implicitly in the $|\epsilon_+(k,\omega)|^2$ factor of $\langle |\rho(k,\omega)|^2 \rangle$.

The Fourier Density Function Theory

For $f_1(v)$ and $f_2(v)$, contour integration in the complex ω-plane is the most convenient way of performing the integrations indicated in equations (20b) and (20c), but the dielectric function must be more precisely defined. The function $\epsilon(k,\omega)$ can be taken to be analytic in either the upper or lower half ω-plane but has a discontinuity along the entire real axis. For the distribution functions being considered, the only resonances in $\rho(k,\omega)$ come from zeros of $\epsilon(k,\omega)$, which occur in the upper half ω-plane. Therefore, the dielectric function was chosen to be analytic in the lower half plane (denoted as

$\epsilon_+(k,\omega)$, where the + sign is carried over from the positive real s half-plane) with analytic continuation into the upper half ω-plane. The function $\epsilon_+(k,\omega)$ is, therefore, an entire function of ω when defined as follows:

$$\epsilon_+(k,\omega) = 1 + \frac{\omega_p^2}{k^2}\int_{-\infty}^{\infty} dv\, \frac{\partial f^0(v)/\partial v}{\frac{\omega}{k} - v} \qquad (\text{Im } \omega < 0) \qquad (21a)$$

$$\epsilon_+(k,\omega) = 1 + \frac{\omega_p^2}{k^2} P\int_{-\infty}^{\infty} dv\, \frac{\partial f^0(v)/\partial v}{\frac{\omega}{k} - v} + i\pi \frac{\omega_p^2}{k^2} \frac{\partial f^0(v)}{\partial v}\Bigg]_{v=\frac{\omega}{k}} \qquad (\text{Im } \omega = 0^-) \qquad (21b)$$

$$\epsilon_+(k,\omega) = 1 + \frac{\omega_p^2}{k^2}\int_{-\infty}^{\infty} dv\, \frac{\partial f^0(v)/\partial v}{\frac{\omega}{k} - v} + 2\pi i \frac{\omega_p^2}{k^2} f^0\left(\frac{\omega}{k}\right) \qquad (\text{Im } \omega > 0) \qquad (21c)$$

In equation (21), Im $\omega = 0^-$ implies the value on the real axis approached from below. By using the Plemelj formulas, $\epsilon_+(k,\omega)$ is seen to be continuous in the entire ω-plane.

Some simplification in evaluating $\langle|\rho(k)|^2\rangle$ can be accomplished by explicitly substituting $f^0(v)$ in $\langle|\rho(k,\omega)|^2\rangle$; that is, with $f^0(v) = Ae^{-\beta v^r}$, then

$$f^0\left(\frac{\omega}{k}\right) = -\frac{1}{r\beta v^{r-1}} \frac{\partial f^0(v)}{\partial v}\Bigg]_{v=\frac{\omega}{k}}$$

If it is noted from equation (21b) that $\frac{\partial f^0(v)}{\partial v}\Big]_{v=\frac{\omega}{k}} = \frac{k^2}{\pi\omega_p^2}\,\text{Im}\,\epsilon(k,\omega)$, then

$$\langle|\rho(k)|^2\rangle = \int_{-\infty}^{\infty} d\omega\, \langle|\rho(k,\omega)|^2\rangle = -n\sigma^2 \frac{k^r}{\pi r\beta\omega_p^2}\int_{-\infty}^{\infty} d\omega\, \frac{1}{\omega^{r-1}} \frac{\text{Im}\,\epsilon(k,\omega)}{|\epsilon(k,\omega)|^2}$$

$$= n\sigma^2 \frac{k^r}{\pi r\beta\omega_p^2}\int_{-\infty}^{\infty} d\omega\, \frac{1}{\omega^{r-1}}\,\text{Im}\left[\frac{1}{\epsilon(k,\omega)}\right] = n\sigma^2 \frac{k^r}{\pi r\beta\omega_p^2} P\int_{-\infty}^{\infty} d\omega\, \frac{1}{\omega^{r-1}}\,\text{Im}\left(\frac{1}{\epsilon}\right) \qquad (22)$$

where the last step follows because any real convergent integral equals its own principal part. This relation may be rewritten as

$$\langle|\rho(k)|^2\rangle = n\sigma^2 \frac{k^r}{\pi r\beta\omega_p^2}\,\text{Im}\, P\int_{-\infty}^{\infty} \frac{1}{\omega^{r-1}}\left[\frac{1}{\epsilon_-(k,\omega)}\right] d\omega = n\sigma^2 \frac{k^r}{\pi r\beta\omega_p^2}\,\text{Im}\, I(k)$$

The integral I(k) may then be evaluated by contour integration along the path shown in figure 4. The path proceeds along the real ω-axis dented along l_ρ into the lower half

ω-plane to avoid the pole of I(k) at $\omega = 0$ and is closed in the lower half-plane along l_∞ where $|\omega| \to \infty$. The integrand is analytic within this contour so the Cauchy residue theorem gives

$$I(k) = P\int_{-\infty}^{\infty} d\omega \frac{1}{\omega^{r-1}}\left[\frac{1}{\epsilon_-(k,\omega)}\right] = -\int_{l_\rho} d\omega \frac{1}{\omega^{r-1}}\frac{1}{[\epsilon(k,\omega)]} - \int_{l_\infty} \frac{d\omega}{\omega^{r-1}}\frac{1}{[\epsilon(k,\omega)]} \qquad (23)$$

The first case to be treated is the Maxwellian distribution, for which $r = 2$ and there is a simple pole at $\omega = 0$. The integral along l_∞ does not vanish in this case but is finite because $\lim_{|\omega|\to\infty} \epsilon(k,\omega) \approx 1$, with deviations of order $\frac{1}{\omega^2}$ (ref. 21). Thus, with $\omega = \rho \exp i\theta$,

$$I(k) = -\pi i\left[\frac{1}{\epsilon_+(k,\omega)}\right]_{\omega=0} - \int_0^{-\pi} i\, d\theta = -\pi i\left[\frac{1}{1 + \frac{\omega_p^2}{k^2}(2\beta)} - 1\right]$$

Using the second moment of the distribution function to show that $\beta_1 = \frac{1}{2v_T^2}$ for $f_1(v)$, together with $D = \frac{v_T}{\omega_p}$, then

$$\left\langle\left|\rho_1(k)\right|^2\right\rangle = n\sigma^2 \frac{k^2D^2}{1 + k^2D^2} \qquad \left(f^0(v) = f_1(v)\right) \qquad (24)$$

For the Druyvesteyn distribution ($r = 4$), the integral along l_∞ vanishes because of the ω^{-3} dependence of the integrand. Considerable care must, however, be taken along the dented contour l_ρ because the contribution from a partially included singularity is generally finite only for a simple pole. The contribution will be finite in this case for several reasons shown subsequently.

In evaluating $\frac{1}{\omega^3} I(k,\omega)$ along l_ρ, where $I(k,\omega) = \frac{1}{\epsilon(k,\omega)}$, the analytic function $I(k,\omega)$ may be expanded in a convergent Taylor series within a radius δ about $\omega = 0$. (Note that this expansion is made possible by the analytic continuation of $\epsilon_+(k,\omega)$ in equation (21).) With $\omega = \rho e^{i\theta}$, then

$$I(k) = -\left[\int_{l_\rho} d\omega \frac{I(k,0)}{\omega^3} + \int_{l_\rho} d\omega \frac{I'(k,0)}{\omega^2} + \int_{l_\rho} d\omega \frac{I''(k,0)}{2\omega} + \cdots\right]$$

$$= -\left\{\lim_{\rho\to 0}\left[\int_\pi^{2\pi} d\theta \frac{i\exp(-2i\theta)}{\rho^2} I(k,0) + \int_\pi^{2\pi} d\theta \frac{e^{i\theta}}{\rho} I'(k,0) + \int_\pi^{2\pi} \frac{i\, d\theta\, I''(k,0)}{2} + \cdots\right]\right\}$$

where

$$I'(k,0) = \left.\frac{dI(k,\omega)}{d\omega}\right]_{\omega=0}$$

$$I''(k,0) = \left.\frac{d^2I(k,\omega)}{d\omega^2}\right]_{\omega=0}$$

The first integral is of the form $\int_{\pi}^{2\pi} e^{-2in\theta}$ which is identically zero. The next term gives, in general, a zero imaginary part but a divergent real part; this term, however, does not contribute to $<|\rho(k)|^2>$ because the imaginary part of $I(k)$ is to be taken. In any case, the odd order derivatives of $I(k,\omega)$ would be zero for any even r (that is, any symmetric distribution function) since odd order derivatives will have odd integrands. The next term contributes $\pi i \frac{I''(k,0)}{2}$ $\left(\text{or, in general, } \pi i \frac{I^{r-2}(k,0)}{(r-2)!}, \text{ the usual residue for a pole of order } r-1\right)$ and the remaining terms go to zero in the limit $\delta \to 0$. For $r = 4$, the result is

$$I(k) = \frac{\pi i}{2}\left\{\frac{1}{\left[\epsilon(k,\omega)\right]^2}\frac{d^2\epsilon(k,\omega)}{d\omega^2}\right\}_{\omega=0} = 4\pi i \frac{\omega_p{}^2\beta}{k^4}$$

If the second moment of the distribution function is used to show that

$$\beta_2 = \frac{1}{v_T{}^4}\left[\frac{\Gamma\left(\frac{3}{4}\right)}{\Gamma\left(\frac{1}{4}\right)}\right]^2$$

where $\Gamma(b)$ denotes the gamma function $\Gamma(b) = \int_0^{\infty} dy\, y^{b-1}\exp(-y)$, then

$$<|\rho_2(k)|^2> = n\sigma^2 \frac{k^4}{\left\{k^2 + \frac{4}{D^2}\left[\frac{\Gamma\left(\frac{3}{4}\right)}{\Gamma\left(\frac{1}{4}\right)}\right]^2\right\}^2} \tag{25}$$

The concept of the Debye distance can be extended to nonequilibrium situations by finding a scale length in the equations whose use is analogous to D. In equation (25) the obvious choice is

$$D_2 = \frac{v_T}{2\omega_p}\left[\frac{\Gamma\left(\frac{1}{4}\right)}{\Gamma\left(\frac{3}{4}\right)}\right] = 1.48D$$

The quantity D_2 is later shown to be analogous to the Debye distance in that it serves as a scale factor for nonequilibrium screening of plasma fields. Equation (25) then simplifies to

$$\left\langle \left|\rho_2(k)\right|^2 \right\rangle = n\sigma^2 \frac{(kD_2)^4}{\left[1 + (kD_2)^2\right]^2} \tag{26}$$

As a final example, $r = \infty$ gives the square distribution $f_3(v)$ shown in figure 2, for which $\left\langle \left|\rho(k,\omega)\right|^2 \right\rangle$ can be integrated directly. If it is noted that

$$f_3(v) = \frac{1}{2a} = \frac{1}{2\sqrt{3}\, v_T}$$

for $|v| < a$ and is zero elsewhere, then

$$\frac{\partial f_3(v)}{\partial v} = \frac{1}{2a}\left[\delta(v + a) - \delta(v - a)\right]$$

If the dispersion relation

$$\omega_k^2 = \omega_p^2 + k^2a^2$$

is used, then

$$\frac{1}{\epsilon(k,\omega)} = 1 + \frac{\omega_p^2}{\omega^2 - \omega_k^2}$$

so that

$$\left\langle \left|\rho_3(k)\right|^2 \right\rangle = \frac{n\sigma^2}{2ak} \int_{-\infty}^{\infty} \left(1 + \frac{\omega_p^2}{\omega^2 - \omega_k^2}\right)^2 d\omega$$

Integration yields

$$\left\langle \left|\rho_3(k)\right|^2 \right\rangle = n\sigma^2 \left[1 + \frac{\omega_p^2}{ka\omega_k} \log\left(\frac{\omega_k - ka}{\omega_k + ka}\right) + \frac{\omega_p^4}{4ka\omega_k^3} \log\left(\frac{\omega_k + ka}{\omega_k - ka}\right) + \frac{\omega_p^2}{2\omega_k^2}\right] \tag{27}$$

With $\Omega = \frac{\omega_p}{\omega_k}$ and an analogous "nonequilibrium Debye distance" $D_3 = \frac{a}{\omega_p} = \sqrt{3}\, D$, equation (27) simplifies to

$$\left\langle \left|\rho_3(k)\right|^2 \right\rangle = n\sigma^2 \left[1 + \frac{\Omega}{kD_3} \log \frac{\sqrt{1 + (kD_3)^2} - kD_3}{\sqrt{1 + (kD_3)^2} + kD_3} \left(1 - \frac{\Omega^2}{4}\right) + \frac{\Omega^2}{2} \right] \tag{28}$$

The Potential Energy Harmonics

Figures 5 and 6 show experimental measurements of $W(k)$, the Fourier harmonics of the total potential energy as a function of kD, a dimensionless wave number for two plasmas having initially Maxwellian $\left[f(v) = f_1(v)\right]$ and square $\left[f(v) = f_3(v)\right]$ distributions, respectively. Implicit in the comparison with theory is the fact that $f_1(v)$ and $f_3(v)$ are considered to be stationary distribution functions; this fact is restricted to one-dimensional plasmas as a result of the first-order kinetic theory considered later. Dawson (ref. 16), in fact, considers transient changes in nonequilibrium distribution functions, but application of these corrections is of limited usefulness in view of the time limitations of Dawson's treatment and the unnecessary complications incurred in using the modified distribution function. All plasmas described in this paper were generated with $N = 1000$ and $\Delta T = 0.1$; the plasmas used to generate the data of figures 5 and 6 both have $nD = 20$. This intermediate value of nD is large enough to allow nonequilibrium effects to be apparent and short enough to allow several modes to occur in the critical range of kD in a stationary state. Using kD, a dimensionless wave number, as the abscissa emphasizes the scale of separation between propagating, coherent oscillations ($kD < 1$) and those disturbances damped out within a few Debye distances ($kD > 1$).

In figure 5, the theoretical curve is obtained from equations (20b) and (24) and is shown as a continuous curve for clarity only. For a finite system size, the potential energy harmonics have meaning only for integral mode numbers c, where $kD = \frac{2\pi cD}{L}$. The data for the Maxwellian plasma agree well with theory except for large fluctuations in the region $kD < 1$; these fluctuations are discussed below. The sum over the first 20 modes shown here does, however, converge to within 10 percent of the predicted sum over these modes.

For the plasma with $f(v) = f_3(v)$ (fig. 6), the theory curves for $f_2(v)$ and $f_3(v)$ calculated from equations (20b), (26), and (28) are both plotted. The term $W_2(k)$ is of interest not only because of its qualitative and quantitative similarity to $W_3(k)$, combined with an analytically simpler form, but also because $W_2(k)$ may be more relevant on physical grounds. As will be shown in the section on relaxation effects, for moderate values of nD, transient relaxation of $f_3(v)$ results in a distribution close to $f_2(v)$ and the specific choice of $W_2(k)$ or $W_3(k)$ depends on scaling of first-order terms and averaging intervals. The scatter of the experimental data also makes any distinction meaningless. The agreement between experiment and theory is acceptable for short

wavelengths ($kD > 1.6$) but below this level not only are fluctuations large but also $W(k)$ does not go to zero with kD; at best, there is some tendency for $W(k)$ to peak at nonzero kD.

There are several possible explanations of these difficulties, some based on limitations of the theory and others due to practicalities of the experiment. Several possibilities are as follows:

(1) The energy balance of the long wavelength modes may be affected by nonlinear coupling not described by the linear theory; that is, the random phase approximation may not be applicable.

(2) Long wavelengths may be excited by random (roundoff) errors in calculation of the particle positions. These errors are basic to the computer program used for these experiments which only approximated by the $\overline{\dot{E}_j}$ term in equation (5b) the time dependency of the electric field during a time step; these errors could be eliminated only by using an exact program which is seriously limited by time considerations for $nD > 10$. Random position errors affect the long wavelengths preferentially, because with $n(x)$ constant (that is, random) $|\rho(k)|^2 = \text{Constant}$; thus,

$$\langle |E(k)|^2 \rangle \propto \frac{\langle |\rho(k)|^2 \rangle}{k^2} = \frac{\text{Constant}}{k^2}$$

which diverges at small k.

However they may be excited, these waves cannot be Landau damped, because, as pointed out by Weitzner (ref. 23), there are no particles with velocities equal to the phase velocity of (that is, synchronous with) the waves. Because of the limited number of particles that can reasonably be treated in the computer experiment, this cutoff is at least as high as $kD \approx 0.3$ and often higher. Also, because there is generally a small number of particles with high velocity, the poor statistics resulting from this scarcity upset the detailed balance of excitation and damping.

(3) The zeroeth-order kinetic theory with which the calculations are compared is not applicable at long wavelengths for finite nD (nonzero graininess); that is, the limits $g \to 0$, $k \to 0$ do not commute. This problem has been investigated by Kaufman (ref. 24) who predicts a finite value of E_k^2 as $kD \to 0$. The potential energy in a given model depends on a balance between excitation and damping to successive orders in the graininess parameter; that is,

$$W(k) \propto \frac{e_0(k) + g e_1(k) + g^2 e_2(k) + \cdots}{d_0(k) + g d_1(k) + g^2 d_2(k) + \cdots}$$

where e_γ and d_γ represent the excitation and damping coefficients to order γ in g. In thermal equilibrium, this condition presents no difficulty because this ratio to each

order is 1/2, and only the fluctuations disturb the long wavelengths. For nonequilibrium plasmas, only the zeroeth-order contribution vanishes and other contributions will go to a finite level.

The first-order contribution to the potential energy comes from collisional effects. By use of a phenomenological model for the collisions, deviation from the zeroeth-order theory is predicted for $kD < (\log_e \lambda)^{-1/2}$ where $\lambda \approx nD$. For $nD = 10$ and 60, the limits of the present experiments, the breakdown of the Vlasov theory comes at ≈ 0.66 and 0.49, respectively; thereby the difficulty of adequately representing the long wavelengths with a plasma of reasonable size (due to the $L/D \gg 1$ restriction) by the Vlasov theory is emphasized. Tripling the upper range of nD (to 180) and taking $N = 3000$ (to maintain the same L/D) should make the Vlasov treatment good down to $kD = 0.44$. The improvement in resolution would hardly be justified in view of the greatly increased calculation time. Difficulties with the zeroeth-order (that is, Vlasov) results in no way prejudice the credibility of first-order results, for it is precisely the effects of nonzero graininess (that is, finite nD) that destroy the correlationless nature of the Vlasov equation. It must be pointed out that this discussion puts the wave amplitude in doubt, but offers no insight into the large fluctuations observed.

(4) Whatever the means of excitation of the long wavelength modes, Dawson (ref. 15) shows that they require progressively longer times to reach a stationary state as $k \to 0$. Physically, Landau damping has been visualized as spontaneous emission of a plasma wave (plasmon) by a fast particle; the resultant energy loss is reflected in a slowing down of the particle (ref. 16). Overall balance is maintained by absorption of the wave by a particle whose velocity is nearly synchronous with the phase velocity of the wave. The scarcity of particles in the high-velocity tail of the distribution function means that statistics on the long wavelengths will be poor; thus, the particular modes of the spectrum appear to be overexcited for long times. As expected, no major change can be seen in the total energy of the system during these fluctuations; energy is conserved, but is not distributed correctly.

Electric-Field Spatial Correlations

Theory.- By integrating over both ω and k, it is possible to smooth the effect of long wavelength fluctuations and yet still retain enough information to distinguish between equilibrium and nonequilibrium results. The spatial correlation of the electric field, that is,

$$C(\lambda,0) = \langle E(x,t)\ E(x+\lambda,t) \rangle_{x,t}$$

results from such an integration. All details of interest are found in the first few Debye lengths, within the limits of applicability of the zeroeth-order theory as outlined by

Kaufman (ref. 24). This function is closely related to the Debye shielding in that the field at a point $x + \lambda$ can be shown to be correlated to the field at a point x, through an exponential-shielding law in which the Debye distance or its analog is the scale length. By using equation (20c), $\overline{C}(\lambda,0)$ is easily evaluated for $f_1(v)$ and $f_2(v)$. For $f_1(v)$,

$$\overline{C_1}(\lambda,0) = \frac{L}{4\pi D^2} \int_{-\infty}^{\infty} \frac{D^2 \exp(ik\lambda)}{1 + k^2 D^2} \, dk$$

Closing the k-axis contour at infinity in the upper half plane gives, from the residue of the pole at $k = +ik_D$,

$$\overline{C_1}(\lambda,0) = \frac{L}{4D} \exp\left(-\frac{\lambda}{D}\right) \tag{29}$$

Evaluation of $\overline{C_2}(\lambda)$ involves a second-order pole. Once again, $D_2 = 1.48D$ is taken as a characteristic scaling distance, so that

$$\overline{C_2}(\lambda,0) = \frac{L}{4\pi D^2} \int_{-\infty}^{\infty} \frac{k^2 D_2{}^4 \exp(ik\lambda)}{\left[1 + \left(kD_2\right)^2\right]^2} \, dk$$

Evaluating the contour in the upper half plane yields

$$\overline{C_2}(\lambda,0) = \frac{LD_2}{8D^2}\left(1 - \frac{\lambda}{D_2}\right) \exp\left(-\frac{\lambda}{D_2}\right) \tag{30}$$

The quantity $\overline{C_2}(\lambda,0)$, which is quantitatively close to $\overline{C_3}(\lambda,0)$ is used for comparison of experimental results. As expected, integrating over k gives a smoother result than $W(k)$, the potential harmonics, because correlations are averaged over more variables.

Measurements.- Figures 7 and 8 show measurements of the variation of $\overline{C}(\lambda,0)$ with λ/D and λ/D_2 for $f_1(v)$ and $f_3(v)$, respectively, where $nD = 20$ for both plasmas. It should be noticed that for $\lambda = 0$, $\overline{C}(\lambda,0)$ reduces to potential energy, and thereby suggests the intepretation of Debye screening as the shielding of potential fields by the dielectric plasma medium.

The behavior of $\overline{C}(\lambda)$ for small values of T is erratic because of the highly artificial state in which the calculations are started. The plasma particles are initially distributed uniformly; electrons and ions alternate at equal separations, and thus only the shortest wavelength is initially excited. As the plasma is released and the proper correlations are established, longer wavelengths are excited (by graininess effects, nonlinear interactions, and so forth) so that the $W(k)$ spectrum fills in from the highest values of k, and gives for all distributions a transient appearance similar to $W_2(k)$.

The resultant form of $\overline{C}(\lambda,0)$ is shown in figure 7(a) for a Maxwellian plasma, together with the theoretical value $\overline{C_1}(\lambda,0)$ (given in eq. (29)).

As correlations are established in the plasma, the $W(k)$ spectrum and, therefore, $\overline{C}(\lambda,0)$ reaches a stationary state characteristic of the average distribution function of the plasma and this state persists as long as the distribution function remains unchanged. For a Maxwellian plasma this stationary state corresponds to the expected Debye-Hückel shielding. Figure 7(b) shows the form of the shielding when the steady state has been reached and gives good agreement with theory; figure 7(c) shows a long-time average. Both spot checks and long-time averages give the correct result, and all times shown are less than the thermalization time for a nonequilibrium distribution.

The experimental data for $f(v) = f_3(v)$ can be compared with $\overline{C_2}(\lambda,0)$ both qualitatively and quantitatively not only because $\left|W_2(k)\right|^2$ closely approximates $\left|W_3(k)\right|^2$, but also on the basis of relaxation effects treated in the next sections. A sequence of measurements similar to figure 7 is shown for the electric-field spatial correlation for $f(v) = f_3(v)$ in figure 8. The expected antishielding (that is, negative correlation) appears after moderate time (fig. 8(b)) and persists on a long-time average. Again, all times shown are less than the thermalization time. The agreement with $\overline{C_2}(\lambda,0)$ is, however, only qualitative. A major factor in the quantitative discrepancy is, once again, the overexcitation of long wavelengths evident in figure 5. Because of this overexcitation, the total potential energy (and, therefore, $\overline{C_3}(\lambda,0)$) is too high, and thereby shifts the entire level of the curve.

FIRST-ORDER THEORY AND MEASUREMENTS

The Test Particle Theory

The concept of the test particle was introduced by Rostoker and Rosenbluth (ref. 25) as a model for treating first-order (graininess) effects in a plasma. If one artificially tags individual particles in the plasma, the kinetics of these particles interacting with the field, or background, summed over the plasma describe the first-order behavior of the plasma. Such tagging of particles is impossible in a laboratory plasma, but the ease with which this can be done in a computer experiment illustrates the great versatility of this technique.

The test particle is described by a distribution function $f_i(v)$ which is a subset of the overall one-particle distribution function; that is, $\sum_i f_i(v) = f(v)$. In three dimensions the Balescu-Lenard equation (ref. 17) is the kinetic equation for the one-particle distribution function to first order in the graininess parameter. Eldridge and Feix (ref. 14) have solved the one-dimensional form of this equation starting from the first-order kinetic

equations (similar to eqs. (12) and (13)) written for the test particle distribution; that is,

$$\frac{\partial f_i(1)}{\partial t} = \frac{\mu_i}{2} \frac{\partial}{\partial v_1} \sum_j \overline{\sigma_j n_j} \int_{-\infty}^{\infty} dx_2 \, dv_2 \, \operatorname{sgn}(x_1 - x_2) \, P_{ij}(1,2) \tag{31}$$

and

$$\left(\frac{\partial}{\partial t} + v_1 \frac{\partial}{\partial x_1} + v_2 \frac{\partial}{\partial x_2} \right) P_{ij}(1,2) + \frac{\mu_i}{2} \int_{\infty}^{\infty} dx_3 \int_{-\infty}^{\infty} dv_3 \sum_h \overline{n_h \sigma_h} \operatorname{sgn}(x_1 - x_3) \frac{\partial f_i(1)}{\partial v_1} P_{jh}(2,3)$$

$$+ \frac{\mu_i}{2} \int_{\infty}^{\infty} dx_3 \int_{-\infty}^{\infty} dv_3 \sum_h \overline{n_h \sigma_h} \operatorname{sgn}(x_2 - x_3) \frac{\partial f_j(2)}{\partial v_2} P_{ih}(1,3) = - \frac{g}{2} \operatorname{sgn}(x_1 - x_2)$$

$$\times \left[\mu_i \overline{\sigma_j} \frac{\partial}{\partial v_1} - \overline{\sigma_i} \mu_j \frac{\partial}{\partial v_2} \right] f_i(1) \, f_j(2) \tag{32}$$

where $\overline{n_h}$ is the normalized density n_h/n_0, where $f(1)$ denotes the one-particle distribution function of particle 1, and so forth.

Collective effects are contained in the pair correlation function $P(1,2)$, the form of which depends on the entire distribution function; because of this dependence, the test particle results emerge as the interaction of discrete particles with a continuum plasma. The two-particle interaction described by this pair function therefore emerges as the lowest order correction in a plasma of finite graininess. In equation (32), $f_j(2)$ is taken to represent the entire plasma with which the test particle (of type i) is interacting.

By using the methods of Lenard (ref. 26), the Fourier transform of equation (32) can be substituted into equation (31); integration over k, the wave number, yields

$$\frac{\partial f_i(1)}{\partial t} = \frac{g}{2\pi} \frac{\partial}{\partial v_1} \left\{ f_i(1) - \frac{\dfrac{\partial f_i(1)}{\partial v_1} \left[\sum_i \dfrac{n_i}{n_0} f_i(1) \right]}{\dfrac{\partial}{\partial v_1} \sum_i \dfrac{n_j}{n_0} f_i(1)} \right\} \arctan \left[\pi \frac{\dfrac{\partial}{\partial v_1} \sum_i \dfrac{n_i}{n_0} f_i(1)}{\displaystyle\int_{-\infty}^{\infty} \frac{\partial v_2}{v_1 - v_2} \sum_j \frac{n_j}{n_0} \frac{\partial f_j(2)}{\partial v_2}} \right] \tag{33}$$

Metaequilibrium

The most striking result of this one-dimensional kinetic equation follows from summing over all test particle species. If both sides of equation (33) are multiplied by $\overline{n_i}$ and summed over i, the two terms in braces $\{ \}$ cancel identically, from which it follows that

$$\frac{\partial}{\partial t}\sum_i \frac{n_i}{n} f_i = 0 \tag{34}$$

and there is no thermalization of the one-particle distribution function to first-order time scale $\tau_1 = \frac{nD}{\omega_p}$. This result holds only for a one-dimensional system, but is valid for both equilibrium and nonequilibrium plasmas and predicts a stationary state or "metaequilibrium" for any initially stable distribution on a time scale $\tau_1 \approx \frac{nD}{\omega_p} << \frac{(nD)^2}{\omega_p}$. This prediction has served as the basis for checking the experiments with $f_3(v)$ against a nonequilibrium theory. If $f_i(1)$ is not summed over the entire distribution function, that is, $f_i(1) \neq f(v)$, changes in the test particle distribution do appear on a first-order time scale, and relaxation effects on the test particle distribution can be calculated and measured.

These results bear some analogy to a one-dimensional gas of particles having only short-range interactions (binary collisions). In one dimension, conservation of energy and momentum dictates that the two partners in a binary collision retain their original velocities or at most swap velocities. If the test particle distribution is the entire one-particle distribution, no net change occurs; however, if only one of the colliding particles is a test particle and its collision partner is a "field" or background particle, changes in the test particle distribution will occur.

In a plasma the interaction is collective (N-body) and makes this result somewhat surprising. First-order effects are, however, similar to the binary collision case in that energy is exchanged between particles by emission of a plasmon wake by test particles, propagation of this wake through the plasma, and reabsorption by another particle of nearly the same velocity (ref. 16). This emission and absorption gives a somewhat binary character to the interaction, whereas the propagation and damping (that is, absorption) mechanisms are collective effects. This process is effectively a "collision in velocity space," and thus carries over the analogy of the hard sphere gas to the metaequilibrium result described. Thermalization is expected to occur in a higher order description of the plasma including ternary correlations – again in similarity to the short-range collision model where three-particle interactions would bring changes in $f(v)$. The same result also follows directly from Balescu-Lenard equation. In three dimensions, changes in the distribution function do occur on a scale τ_1 by interaction of plasmons of wave vector $\vec{k}$ with test particles for which $\vec{k} \cdot \left(\vec{v}_1 - \vec{v}_2\right) = 0$. The Fourier transform of the interaction potential is the same for one and three dimensions; thus, the equation may be one-dimensionalized by dropping the vector sign and changing a multiplicative constant (ref. 14). In one dimension, the wave vector is always parallel to particle velocities; thus, $\frac{\partial f_i(v)}{\partial t} = 0$ if $f_i(v) = f(v)$.

The persistence of the metaequilibrium is shown in figure 9 for four plasmas with initial velocity distributions of the form $f_3(v)$ and values of nD of 10, 20, 40, and 60; all four velocity distributions are shown at a first-order time $\tau_1 = \frac{nD}{\omega_p} = 4$. The dashed curve represents an equilibrium (that is, Maxwellian) distribution having the same energy and the corners marked at $V = \pm 1.7$ show the corners of the original square. In all cases, $\tau_1 = 4$ is much greater than the zeroeth-order time scale ω_p^{-1}; thus, qualitative differences between the plasmas at τ_1 are the result of secondary and possibly higher order effects.

For $nD = 10$, $\tau = 4 = 0.4\tau_2$ where $\tau_2 = \frac{(nD)^2}{\omega_p}$ and the plasma has already substantially thermalized. In contrast to this, for $nD = 60$, $\tau = 4 = 0.06\tau_2$ (that is, $<<\tau_2$) and the original square shape is well retained. The changes that do occur, however, appear to be most rapid in the high velocity tail of the distribution, which tends to overexcite the long wavelength modes of potential energy; this overexcitation, to some extent, may explain the difficulty in obtaining quantitative agreement for $|\rho(k)|^2$ and $C(\lambda)$. All distributions are modified from their original shape and, for example, for $nD = 20$, $f(v)$ is very close to $f_2(v)$ which, as pointed out earlier, appears to be an intermediate form of $f_3(v)$ in its eventual thermalization.

Relaxation of Test Particles

If $f_i(1)$ is taken as a subgroup of the total distribution, for example, all particles with velocities V_i such that $V_1 - \Delta V \leq V_i \leq V_1 + \Delta V$, $\frac{\partial f_i(1)}{\partial t} \neq 0$ and equation (33) can be viewed as a Fokker-Planck equation of the form

$$\frac{\partial f_i(1)}{\partial t} + \frac{\partial}{\partial v}\left[\chi(v)\, f_i(1) - \frac{1}{2}\frac{\partial}{\partial v}\psi(v)\, f_i(1)\right] = 0 \tag{35}$$

in which $\chi(v) = \frac{\Delta <v_i>}{\Delta t}$ is the drag and $\psi(v) = \frac{\Delta\left(<v_i^2> - <v_i>^2\right)}{\Delta t}$ is the velocity diffusion coefficient. Such a test particle distribution is shown at initial time in figure 10(a) with its parent distribution $f(v)$ (that is, the total velocity distribution at the same time). In this example, $V_1 = 0.4$, $\Delta V = 0.05$, and the parent distribution was initially a square $[f(v) = f_3(v);\ nD = 20]$ whose corners are shown at $V = \pm 1.7$. As time progresses, the test particle distribution interacts with $f(v)$ and changes as shown in figures 10(b) and 10(c). The amplitudes of the time-averaged test particle distributions are amplified by factors of 15 and 25, respectively, in figures 10(b) and 10(c) to aid visual comparison with the parent distribution.

Most of the particles seen by the test group have velocities $< V_1$; thus, the drag experienced by $f_i(v)$ makes $<V_i>$ tend toward zero. This is true, however, only on

the average, and individual members of the group gain or lose more energy than the group average; this condition leads to dispersion or "diffusion" in velocity space. Both effects are indicated in figure 10(b). This dispersion in no way represents the effects of propagating errors in the calculations but is the expected microscopic behavior. After many plasma periods the test particles have relaxed to a stationary state which is not Maxwellian but a duplicate of (that is, synchronized with) the parent distribution. The slight discrepancy between $f(v)$ and $f_i(1)$ in figure 10(c) is due to a slight shift in $f_i(v)$ arising from nonzero $<V_i>$; in this case $<V_i> = 0.1$. This result again supports the metaequilibrium concept in that the test group has not really "thermalized" (in the sense of becoming Maxwellian) but relaxes to a stationary nonequilibrium form.

The exact form of the distribution function is more closely examined in figure 11. In figure 11(a) the parent velocity distribution is plotted with the theoretical curves for the square, Druyvesteyn, and Maxwellian distributions. (Once again, only the outline corners of the square are shown.) The departure from the initial square is evident, but the plasma has not yet become Maxwellian. The relatively good fit to the Druyvesteyn gives more quantitative justification for using the theory for $f_2(v)$ with the zeroeth-order experiments. Figure 11(b) compares the test particle distribution with the theory curve for $f_2(v)$. The test particle distribution $f_i(v)$ shows more fluctuations than $f(v)$ but, once again, $f_2(v)$ provides a reasonable fit.

Diffusion Coefficients

Theory.- Quantitative checks of the first-order kinetic theory are, to some extent, better than those of the zeroeth-order theory. The diffusion of a test particle can be calculated in a very general way by following the work of Thompson and Hubbard (refs. 27 and 28). The equation of motion for the test particle is

$$\dot{v}_i = -\frac{\sigma_i}{m} E_i(t)$$

where $E_i(t)$ is viewed as the stochastic field caused by the rest of the plasma as seen by particle i. For short times, the differential motion is given by

$$\Delta v_i = -\frac{\sigma_i}{m}\int_0^{t_1} E_i\left[x(t - s),\ t - s\right]ds \tag{36}$$

and results in a diffusion coefficient

$$\psi(v) = \psi_{ii}(v) = \frac{d}{dt}<\Delta v_i\ \Delta v_i> = 2<\dot{v}_i\ \Delta v_i> = 2\left(\frac{\sigma_i}{m}\right)^2 <\int_0^{t_1} ds\left\{E_i(x,t)\ E_i\left[x(t - s),\ t - s\right]\right\}> \tag{37}$$

The time over which the correlations persist is short compared with the time during which a particle trajectory is significantly modified; thus, $x(t - s) \approx x(t) - vs$ where v is the average particle velocity. Equation (37) then assumes the form of the autocorrelation coefficient $C(\lambda,\tau)$ with $\lambda = vs$ and $\tau = s$. The short correlation time also permits the upper limit of the s-integration to be extended to infinity, and, as a result,

$$\psi(v) = 2\left(\frac{\sigma_i}{m}\right)^2 \int_{-\infty}^{\infty} dk \int_{-\infty}^{\infty} d\omega \int_{0}^{\infty} ds \, \frac{1}{2\pi} < \left|E(k,\omega)\right|^2 > \exp i(kv + \omega)s$$

$$= 2\left(\frac{\sigma_i}{m}\right)^2 \int_{-\infty}^{\infty} dk \int_{-\infty}^{\infty} d\omega \int_{-\infty}^{\infty} ds \, H(s) \, \frac{1}{2\pi} < \left|E(k,\omega)\right|^2 > \exp i(kv + \omega)s$$

where $H(s)$ is the Heaviside unit step function. Performing the s-integration yields

$$\psi(v) = \left(\frac{\sigma_i}{m}\right)^2 \int_{-\infty}^{\infty} d\omega \int_{-\infty}^{\infty} dk < \left|E(k,\omega)\right|^2 > \delta(kv + \omega) \tag{38}$$

In terms of the dimensionless velocity $V = \frac{v}{v_T}$ and the first-order scaling time $\tau_1 = \frac{nD}{\omega_p}$, one obtains a normalized diffusion coefficient

$$\bar{\psi}(V) = \frac{d}{d\tau_1}\left[< V^2 > - < V >^2\right] = \frac{\omega_p^2}{v_T} \int_{-\infty}^{\infty} d\omega \int_{-\infty}^{\infty} dk \, \frac{f\left(\frac{\omega}{k}\right)}{\left|k^3\right| \left|\epsilon_+(k,\omega)\right|^2} \delta(\omega + kv) \tag{39}$$

The simplest case to treat is $V_1 = 0$, for which the drag, a velocity-dependent force, goes to zero. (Because of the experimental necessity of nonzero ΔV around V_1, the dependence of drag on V introduces additional scattering not strictly due to diffusion. This effect could be more pronounced for $V_1 \neq 0$.) The integration over ω for $V_1 = 0$ then reduces to evaluation of $< \left|E(k,\omega)\right|^2 >$ at $\omega = 0$; that is,

$$\bar{\psi}(V) = \frac{\omega_p^2}{v_T} \int_{-\infty}^{\infty} \frac{f(0)}{\left|k^3\right| \left|\epsilon(k,0)\right|^2} dk = \frac{\omega_p^2}{v_T} \int_{-\infty}^{\infty} \frac{A}{\left|k^3\right| \left|\epsilon(k,0)\right|^2} dk \tag{40}$$

where $f(0) = A$. For $f_1 = A_1 \exp\left(-\beta_1 v^2\right)$,

$$\epsilon(k,\omega=0) = 1 + \frac{\omega_p^2}{k^2} P \int_{-\infty}^{\infty} \frac{df/dv}{0 - v} dv + 0 = 1 + \frac{1}{k^2 D^2} \tag{41}$$

so that with $A_1 = \frac{1}{\sqrt{2\pi} v_T}$,

$$\overline{\psi_1}(V) = \frac{2\omega_p^2}{\sqrt{2\pi}\, n v_T^3} \int_0^\infty \frac{k^4 D^4}{\left(1 + k^2 D^2\right)^2 |k|^2}\, dk = \frac{2\omega_p^2}{\sqrt{2\pi}} = 0.4 \tag{42}$$

Similarly, for $f_2(v) = A_2 \exp\left(-\beta_2 v^4\right)$ where A_2 is defined as

$$A_2 = \frac{2\beta_2^{1/4}}{\Gamma\left(\frac{1}{4}\right)} = \frac{2}{v_T} \frac{\left[\Gamma\left(\frac{3}{4}\right)\right]^{1/2}}{\left[\Gamma\left(\frac{3}{4}\right)\right]^{3/2}}$$

and β_2 is defined preceding equation (25), then

$$\epsilon(k,\omega=0) = 1 + \frac{1}{k^2 D_2^2} \tag{43}$$

where $D_2 = 1.48D$. From this relation,

$$\overline{\psi_2}(V) = \frac{1}{2} \frac{\left[\Gamma\left(\frac{1}{4}\right)\right]^{1/2}}{\left[\Gamma\left(\frac{3}{4}\right)\right]^{3/2}} = 0.687 \tag{44}$$

Finally, for $F_3 = \frac{1}{2a}$ for $|v| < a = 3v_T$,

$$\epsilon(k,\omega=0) = \frac{1}{1 + \left(\frac{1}{kD_3}\right)^2} \tag{45}$$

and $D_3^2 = \left(\frac{a}{\omega_p}\right)^2$; thus,

$$\overline{\psi_3}(V) = \frac{\sqrt{3}}{2} = 0.866 \tag{46}$$

Measurements.- The experimental results of test particle diffusion calculations are shown in figures 12 and 13. By selecting the test particles in each plasma approximately three plasma periods after the initiation of the experiment $\left(T_0 = 20\omega_p^{-1}\right)$, the variance of the velocity is plotted as a function of time in units of the zeroeth-order time scale (that is $\tau_0 = \omega_p t$) for four plasmas having $nD = 10$, 20, 40, and 60 for an equilibrium plasma (fig. 12) and a nonequilibrium plasma, $f(v) = f_3$ (fig. 13). The initial slope of these lines gives the desired diffusion coefficient; in taking the slope, the relaxation time $\frac{t}{\tau_1} = \frac{\omega_p t}{nD}$ must be used, rather than the zeroeth-order time scale on which the data are

plotted for clarity. The initial slopes given in table I for the equilibrium plasma are relatively independent of nD and check well with the theoretical value of 0.4. The nonequilibrium case, which in figure 11 showed increasing stability of the metaequilibrium with increasing nD, again shows the effect of nD on the thermalization time. For $nD = 10$, the substantial thermalization suggested in figure 11 is borne out by a diffusion coefficient of 0.5 which is close to the equilibrium value of 0.4. The relative stability of the initial square for $nD = 60$ (fig. 11) is reflected in a diffusion coefficient of 0.9 compared with the theoretical value of 0.86 for $f_3(v)$. For $nD = 20$, the diffusion coefficient of 0.65 indicates partial thermalization; the proximity of this value to the theoretical value of 0.70 for $f_2(v)$ again justifies the use of $\left|E_2(k)\right|^2$ and $\overline{C_2}(\lambda,0)$ theory for experiments with $f_3(v)$. The diffusion measurements are summarized in table I.

Drag Coefficient Measurements

Figure 14 shows drag measurements on the same four equilibrium plasmas studied. The average velocity of the three test groups $\left(<V_1>_0 = 0.4,\ 1.0,\ \text{and}\ 1.4\right)$ is shown as a function of normalized time $\tau_1 = \frac{\omega_p t}{nD}$; the drag coefficient is given as the slope of the curves, and the straight lines represent the theoretical values calculated in reference 12 from equation (33). The data generally agree with the theory except for the fluctuations in the $nD = 40$, $V_1 = 1.0$ case. Figure 15 shows on a much longer time scale the relaxation of test particles initially at the thermal velocity. The extensive overlap of the data, even down to very small velocities, verifies the correctness of the relaxation time scale τ_1, because the zeroeth-order times $\left(\text{that is, } \omega_p t\right)$ used for the generation of the plasma vary by a factor of 6 as nD goes from 10 to 60.

The data for $f_3(v)$ are more scattered, but generally exhibit the trend shown in figure 16 for $V_1 = 1.0$, where the straight line again represents the equilibrium drag. The thermalization of the plasma for which $nD = 10$ is again shown by its agreement with the equilibrium line. For $nD = 20$, 40, and 60, the drag (that is, slope of the data) is greater than that for the Maxwellian, as would be expected from equation (35). Figure 17 again shows the consistency of the long-time scaled behavior of the drag for the four plasmas considered.

CONCLUSIONS

In conclusion, an approximate, self-consistent N-body calculation has been used to study the microscopic behavior of one-dimensional plasmas in a controllable, physically realistic manner. The physical consistency (for example, energy conservation) in the approximate model improves as nD (particle density times Debye distance) increases because of smoothing of the graininess effects even though more crossings occur per fixed time step. A large range of values of the graininess parameter g has permitted

separation of collective and individual particle effects through the zeroeth- and first-order theory.

By using the Vlasov theory, calculations of $W(k)$, the Fourier harmonics of the potential energy, give good agreement for equilibrium plasmas, but only fair agreement for nonequilibrium. The balance of long wavelength modes is probably not well described by the Vlasov theory for finite g and in this range, even the equilibrium agreement may be fortuitous. Integrating over wavelength, the electric field spatial correlation $\overline{C}(\lambda)$ shows excellent agreement in equilibrium and qualitative agreement out of equilibrium; in particular, antishielding is observed as a stationary effect for a range of several Debye lengths.

The metaequilibrium or stationarity of nonequilibrium distributions was verified and serves as the basis for study of nonequilibrium plasmas. The test particle approach is used for calculation of first-order effects and produces good agreement with the expected drag and velocity diffusion. The diffusion coefficient is shown to be a good indication of the extent of thermalization in a nonequilibrium plasma.

Langley Research Center,
National Aeronautics and Space Administration,
Langley Station, Hampton, Va., June 13, 1968,
129-02-01-01-23.

APPENDIX

GENERAL DESCRIPTION OF THE COMPUTER PROGRAMS

The data in this report have been generated by three separate computer programs. Program I generates the time history of the particle motions in a one-dimensional, self-consistent electrostatic plasma. Program II uses the position data from program I to calculate the Fourier modes of the potential energy and the Debye screening. Program III uses the velocity data from program I to give the total and test particle distribution functions and the drag and velocity diffusion coefficients.

The data from program I, in the form of position, velocity, and particle order arrays for successive time steps (that is, cycles) are output on magnetic tape to facilitate their later use with programs II and III. Kinetic and potential energy and total momentum are also output at each cycle and serve as checks on self-consistency and disaster monitors. By using three separate programs, the diagnostic parameters of programs II and III may readily be changed without repeating the relatively time-consuming trajectory calculation.

In program I, equations (5a) and (5b) are used to calculate the positions and velocities of identified particles in a stepwise manner; that is, the $x_j(T_1 + \Delta T)$ of one cycle becomes the $x_j(T)$ for the next cycle. The electric field is calculated using equation (2b) (a sum of $N + 1$ terms) rather than equation (2a) (a sum of $N(N + 1)$ terms) to compute the field seen by each particle. The sole disadvantage of this method is the required generation and storage of a particle-order array in which the identification number of all the particles are stored in order of increasing position value from $x = 0$ to $x = L$. At the end of each cycle, the particle order is established by using a subroutine in which the order from the previous cycle is used as an approximation to the new order. If $\Delta T \ll 1$, few crossings will have taken place and only minor rearrangement is necessary.

The initial particle velocities should be assigned with a random number generator to avoid any correlation between position and velocity, which would be unrealistic. The initial positions should, however, be assigned in a regular manner to avoid large excesses of potential energy. As pointed out in the discussion on potential energy harmonics, a completely random distribution of charge gives far too much potential energy at long wavelengths. This situation increases the time necessary for proper correlations to be established in the plasma because long wavelengths are weakly damped. Regular initial ordering of the particles provides precise control on the initial potential energy which may be concentrated on any wavelength or combination thereof, rather than on the shortest wavelength, as was done in these experiments. The transfer of potential energy from one wavelength to another is an interesting problem in itself.

Program II uses the tape output from program I as input to calculate the Fourier modes of potential energy and the spatial correlation of the electric field. The particles

(that is, sheets) are taken to be infinitely thin so that the symmetric Fourier transform of the charge density at time T is given as

$$\rho(k,T) = \sqrt{\frac{1}{L}} \int_0^L dx\, e^{ikx} \sum_{j=1}^{N} \sigma_j\, \delta\left[x - x_j(T)\right] = \sqrt{\frac{1}{L}} \sum_{j=1}^{N} \sigma_j\, e^{ikx_j(T)}$$

where σ_j and $x_j(T)$ denote the charge and position (at time T) of the jth particle and the wave number is $k = \frac{2\pi c}{L}$. The total potential energy modes are, therefore,

$$W(k) = \frac{\Delta T'}{T_2 - T_1} \frac{1}{2D^2} \sum_{T=T_1}^{T_2} \sum_{j=1}^{N} \sigma_j \left[\cos^2 kx_j(T) + \sin^2 kx_j(T)\right]$$

where $\Delta T'$ is the time interval between samples of $W(k)$. The extent of the time average (that is, $T_2 - T_1$) depends on the wave numbers being investigated because the Landau damping goes to zero with k; thus long wavelengths take longer to come to equilibrium. A minimum averaging time of $\tau_1 = \frac{nD}{\omega_p}$ was used in all calculations and one needs no more than one calculation of $W(k)$ in a time $1/\omega_p$ if redundancy is to be avoided. Accuracy at long wavelengths is still limited, however, by required averaging times which can become of the order of τ_2, in which time the nonequilibrium spectrum changes, and thereby voids the calculation. Also, random position errors inherent in an approximate program continually lead to anomalous excitation of long wavelengths, and make the problem of obtaining good statistics on long wavelengths even more difficult.

The calculation of the electric-field spatial correlation is straightforward. By using the particle order data output by program I, the electric field is calculated at regular intervals from $x = 0$ to $x = L$. If the basic interval is ℓ and λ is some multiple of ℓ, then

$$C(\lambda,0) = \frac{\Delta T'}{T_2 - T_1} \frac{1}{2D^2} \sum_{T=T_1}^{T_2} \sum_{n=0}^{n_{max}} E(n\ell,T)\, E(n\ell + \lambda,T)$$

where n_{max} is the integer part of $(L - \lambda/\ell)$. A slightly modified version of this program has been used by Massel (ref. 29) to calculate the spatial and temporal correlations of potential fluctuations.

Program III provides the most sensitive diagnostics on the approach to equilibrium in the one-dimensional plasma. The overall distribution function is calculated by sorting the velocity arrays. The problem of time averaging is, however, a delicate one and care must be taken in interpreting the error (that is, standard deviation) in the measurements. The first-order relaxation time τ_1 defines the time for statistical independence of measurements of $f(v)$. If, for example, n independent measurements each yield m_i

counts in a given velocity interval, then the probable error in the measurements is $\sqrt{N(v)} = \sqrt{\sum_{i=1}^{n} m_i}$. Thus measurements of $f(v)$ should be separated by times $>\tau_1$.

Because the distribution function thermalizes in a time τ_2, one must also require that all components of an average be taken in a time $\ll \tau_2$. It is often difficult to satisfy both requirements; thus several measurements must be taken within a time τ_1, at the expense of incurring a larger measurement error because the samples are not independent. At the very worst, if all the samples were completely dependent, the error would be $\sqrt{nN(v)} = \sqrt{n^2 \sum_{i=1}^{n} m_i} = n\sqrt{\sum_{i=1}^{n} m_i}$. The actual error is between these two values, but for small nD plasmas, one can expect rather marginal improvement from time averaging.

Measurement of the diffusion and drag coefficients is made with the same sorting and averaging technique as used for the total distribution function. By selecting particles within a narrow velocity interval, the mean and variance of the test particle distribution as a function of time yields the drag and diffusion. If groups in the same velocity range are selected at different times T, the averaged test particle distribution as a function of τ (the time elapsed since selection) is given as

$$f_i(V,\tau) = \frac{\Delta T'}{T_2 - T_1} \sum_{T=T_1}^{T_2} f_i(V, T + \tau)$$

For a test particle calculation, however, statistical independence is achieved more rapidly because the particles are identified. To see why independence is achieved more rapidly, consider the changes produced by a one-dimensional binary collision in which the two particles either swap velocities or reverse the signs of their velocities, because of conservation requirements. Such an interaction changes nothing in the overall distribution function because only the quantity of particles in a velocity interval is noted. If the particles are identified, as in a test-particle calculation, the state of the sample has changed and some degree of independence is attained. Because the number of test particles is a small fraction of the field particles, with which almost all interactions occur, the time for statistical independence of samples should probably be reduced by a factor depending on the ratio of field particles to test particles. Thus, the expected accuracy of a test-particle calculation can be very high, even with closely spaced samples.

REFERENCES

1. Alder, B. J.; and Wainwright, T. E.: Studies in Molecular Dynamics. I. General Method. J. Chem. Phys., vol. 31, no. 2, Aug. 1959, pp. 459-466. II. Behavior of a Small Number of Elastic Spheres. J. Chem. Phys., vol. 33, no. 5, Nov. 1960, pp. 1439-1451.

2. Lomax, R. J.: Transient Space-Charge Flow. J. Electronics Control, vol. 9, no. 2, Aug. 1960, pp. 127-146.

3. Birdsall, Charles K.; and Bridges, William B.: Space-Charge Instabilities in Electron Diodes and Plasma Converters. J. Appl. Phys., vol. 32, no. 12, Dec. 1961, pp. 2611-2618.

4. Bridges, William B.; and Birdsall, Charles K.: Space-Charge Instabilities in Electron Diodes. II. J. Appl. Phys., vol. 34, no. 10, Oct. 1963, pp. 2946-2955.

5. Burger, Peter: The Opposite-Stream Plasma Diode. SEL-64-012 (NASA Grant NsG 299-63), Stanford Univ., Apr. 1964.

6. Buneman, O.: Dissipation of Currents in Ionized Media. Phys. Rev., Second ser., vol. 115, no. 3, Aug. 1, 1959, pp. 503-517.

7. Goldstein, Charles M.: Electron Flow in Low-Density Argon Gas Including Space-Charge and Elastic Collisions. NASA TN D-4087, 1967.

8. Hasegawa, Akira; and Birdsall, Charles K.: Sheet-Current Plasma Model for Ion-Cyclotron Waves. Phys. Fluids, vol. 7, no. 10, Oct. 1964, pp. 1590-1600.

9. Dawson, J. M.: Investigations of Nonlinear Behavior in One-Dimensional Plasma Model. Symposium on Computer Simulation of Plasma and Many-Body Problems, NASA SP-153, 1967, pp. 25-30.

10. Buneman, O.; and Kooyers, G.: Computer Simulation of the Electron Mixing Mechanism in Ion Propulsion. AIAA J., vol. 1, no. 11, Nov. 1963, pp. 2525-2528.

11. Yu, S. P.; Kooyers, G. P.; and Buneman, O.: Time-Dependent Computer Analysis of Electron-Wave Interaction in Crossed Fields. J. Appl. Phys., vol. 36, no. 8, Aug. 1965, pp. 2550-2559.

12. Anon.: Symposium on Computer Simulation of Plasma and Many-Body Problems. NASA SP-153, 1967.

13. Eldridge, O. C.; and Feix, M.: One-Dimensional Plasma Model at Thermodynamic Equilibrium. Phys. Fluids, vol. 5, no. 9, Sept. 1962, pp. 1076-1080.

14. Eldridge, O. C.; and Feix, M.: Numerical Experiments With a Plasma Model. Phys. Fluids, vol. 6, no. 3, Mar. 1963, pp. 398-406.

15. Dawson, John: One-Dimensional Plasma Model. Phys. Fluids, vol. 5, no. 4, Apr. 1962, pp. 445-459.

16. Dawson, John M.: Thermal Relaxation in a One-Species, One-Dimensional Plasma. Phys. Fluids, vol. 7, no. 3, Mar. 1964, pp. 419-425.

17. Montgomery, D. C.; and Tidman, D. A.: Plasma Kinetic Theory. McGraw-Hill Book Co., Inc., c.1964.

18. Smith, Craig; and Dawson, John: Some Computer Experiments With a One-Dimensional Plasma Model. MATT-151 (Contract No. AT(30-1)-1238), U.S. At. Energy Com., Jan. 1963.

19. Landau, L.: On the Vibrations of the Electronic Plasma. J. Phys. (U.S.S.R.), vol. 10, 1946, p. 25.

20. Jackson, J. D.: Longitudinal Plasma Oscillations. J. Nucl. Energy: Pt. C, vol. 1, no. 4, July 1960, pp. 171-189.

21. Rostoker, Norman: Fluctuations of a Plasma (I). Nucl. Fusion, vol. 1, no. 2, Mar. 1961, pp. 101-120.

22. Feix, Marc R.; and von Hagenow, Karl: Connection Between Correlations and Fluctuations in a Plasma. Phys. Fluids (Res. Notes), vol. 8, no. 8, Aug. 1965, pp. 1565-1567.

23. Weitzner, Harold: Plasma Oscillations and Landau Damping. Phys. Fluids, vol. 6, no. 8, Aug. 1963, pp. 1123-1127.

24. Kaufman, Allan N.: Extension of the Plasma Kinetic Equation to Small Wave Numbers. Phys. Rev. Letters, vol. 17, no. 22, Nov. 28, 1966, pp. 1127-1129.

25. Rostoker, Norman; and Rosenbluth, M. N.: Test Particles in a Completely Ionized Plasma. Phys. Fluids, vol. 3, no. 1, Jan.-Feb. 1960, pp. 1-14.

26. Lenard, Andrew: On Bogoliubov's Kinetic Equation for a Spatially Homogeneous Plasma. Ann. Phys., vol. 10, no. 3, July 1960, pp. 390-400.

27. Thompson, W. B.; and Hubbard, J.: Long-Range Forces and the Diffusion Coefficients of a Plasma. Rev. Modern Phys., vol. 32, no. 4, Oct. 1960, pp. 714-718.

28. Hubbard, J.: The Friction and Diffusion Coefficients of the Fokker-Planck Equation in a Plasma. Proc. Roy. Soc. (London), ser. A, vol. 260, no. 1300, Feb. 7, 1961, pp. 114-126.

29. Massel, Gary Alan: The Kinetic Theory of Forced Oscillations in Plasmas. Ph. D. Thesis, North Carolina State Univ., 1967.

TABLE I.- DIFFUSION COEFFICIENT FOR ZERO VELOCITY TEST PARTICLES

nD	$\psi(v)$ for –				
	Theory $f_1(v)$	Experiment $f_1(v)$	Theory $f_3(v)$	Theory $f_2(v)$	Experiment $f_3(v)$
10	0.40	0.37	0.86	0.70	0.48
20	.40	.42	.86	.70	.65
40	.40	.42	.86	.70	.91
60	.40	.41	.86	.70	.90

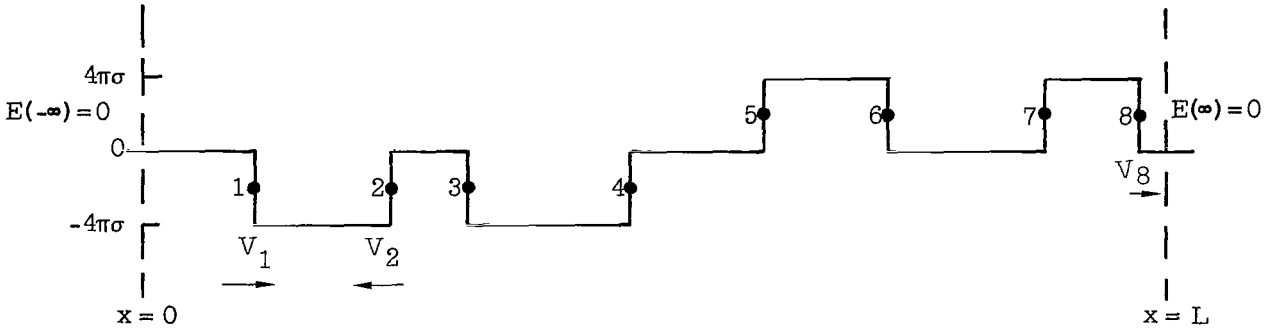

(a) Field before crossings.

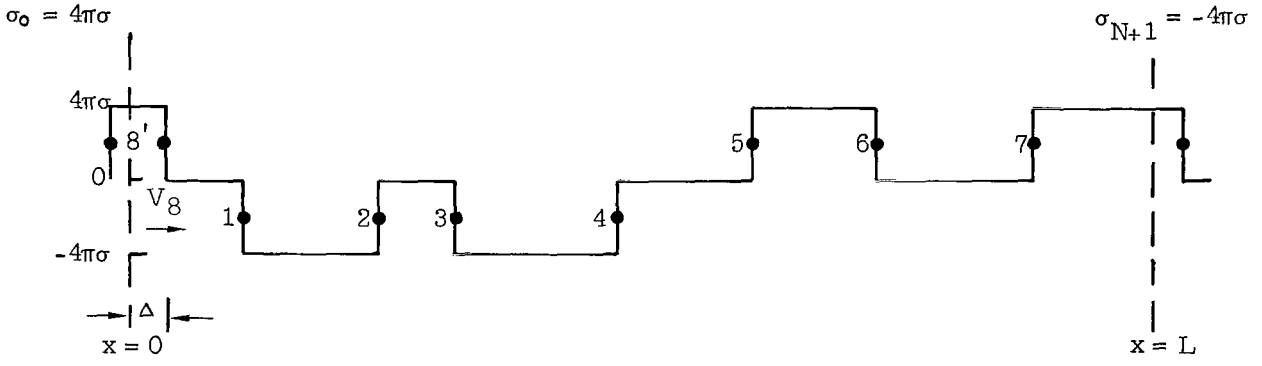

(b) Field after boundary crossing.

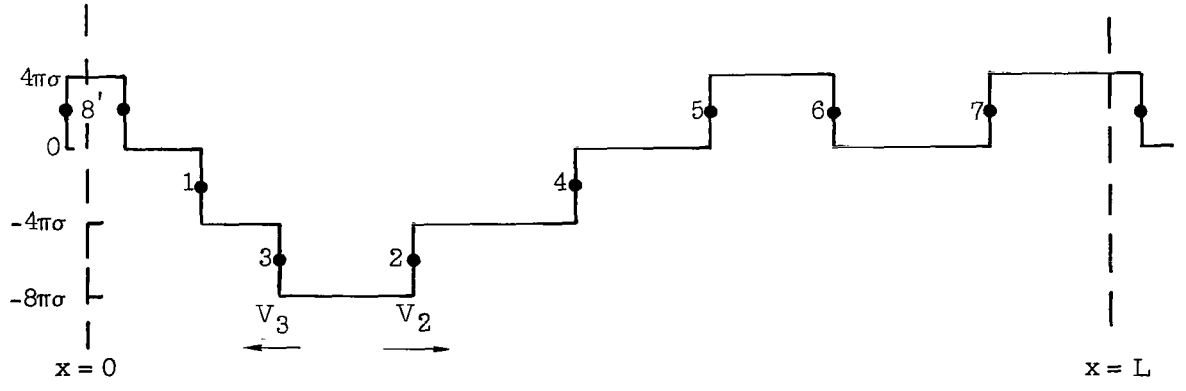

(c) Field after crossing in interval.

Figure 1.- Electric field in sheet model.

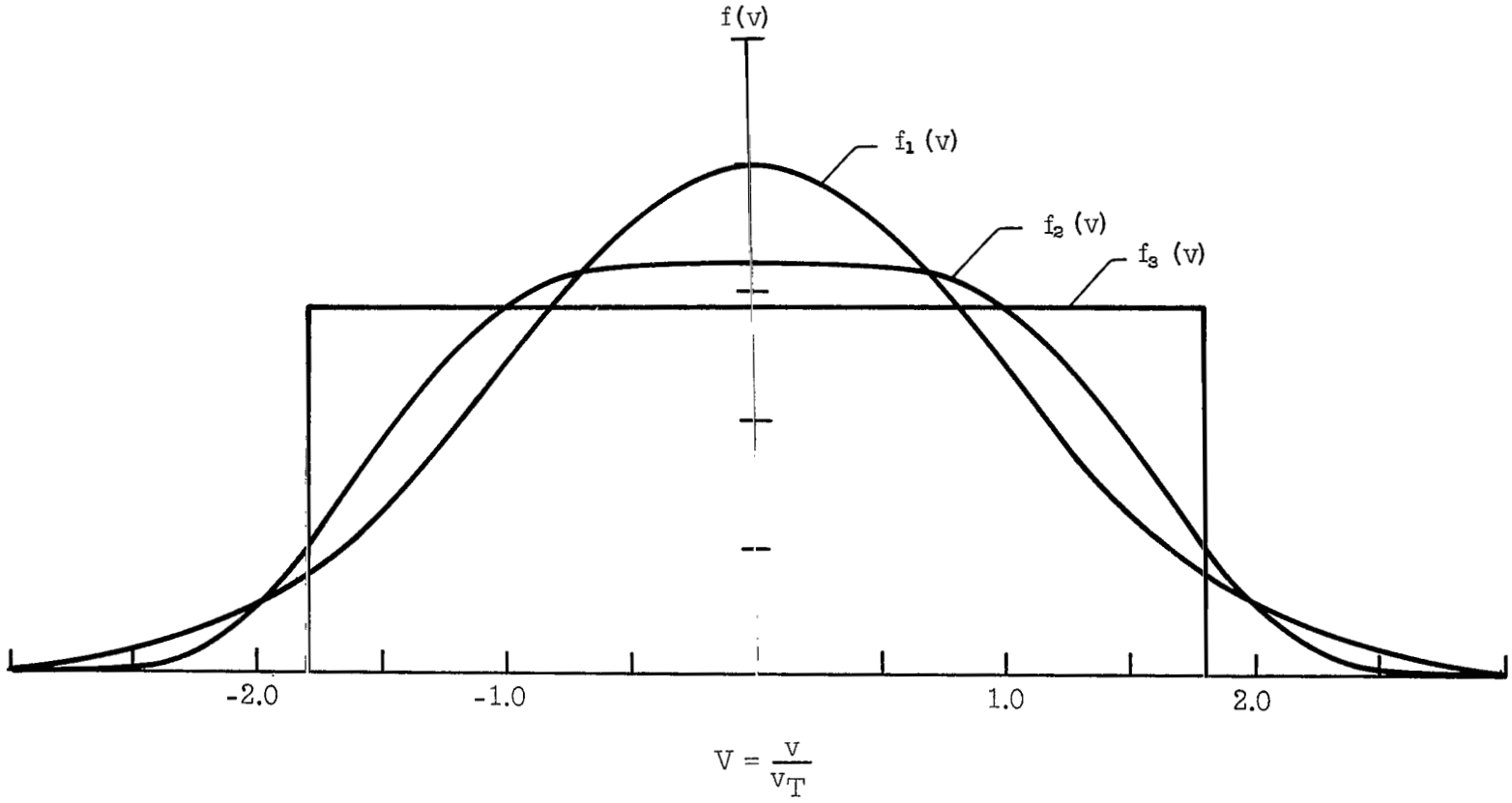

Figure 2.- Input velocity distribution functions. $f_1(v) = A_1 \exp(-\beta_1 v^2)$; $f_2(v) = A_2 \exp(-\beta_2 v^4)$; $f_3(v) = A_3$ for $|v| \leq a$; and $f_3(v) = 0$ for $|v| > a$.

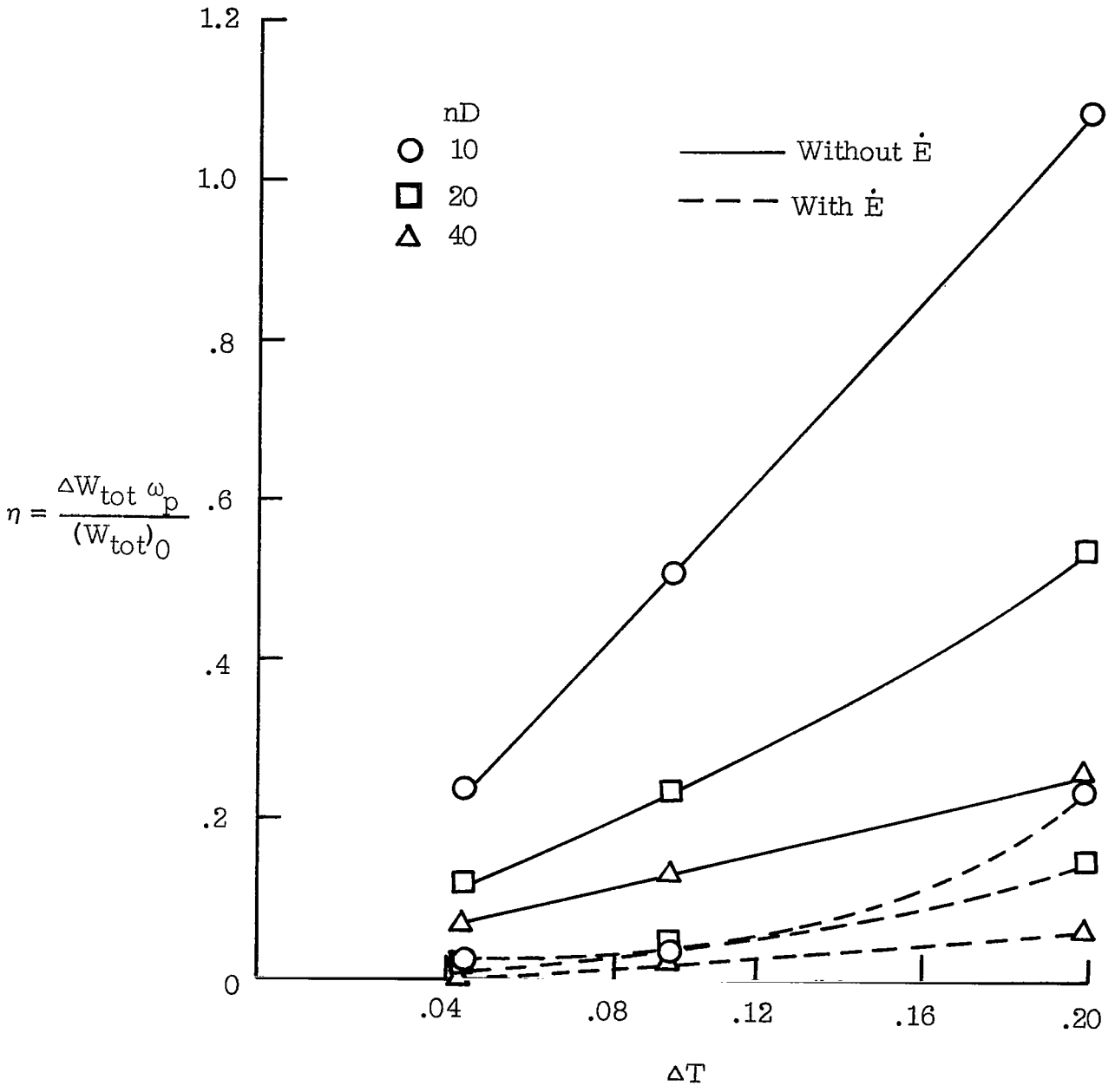

Figure 3.- Fractional energy gain per ω_p^{-1}.

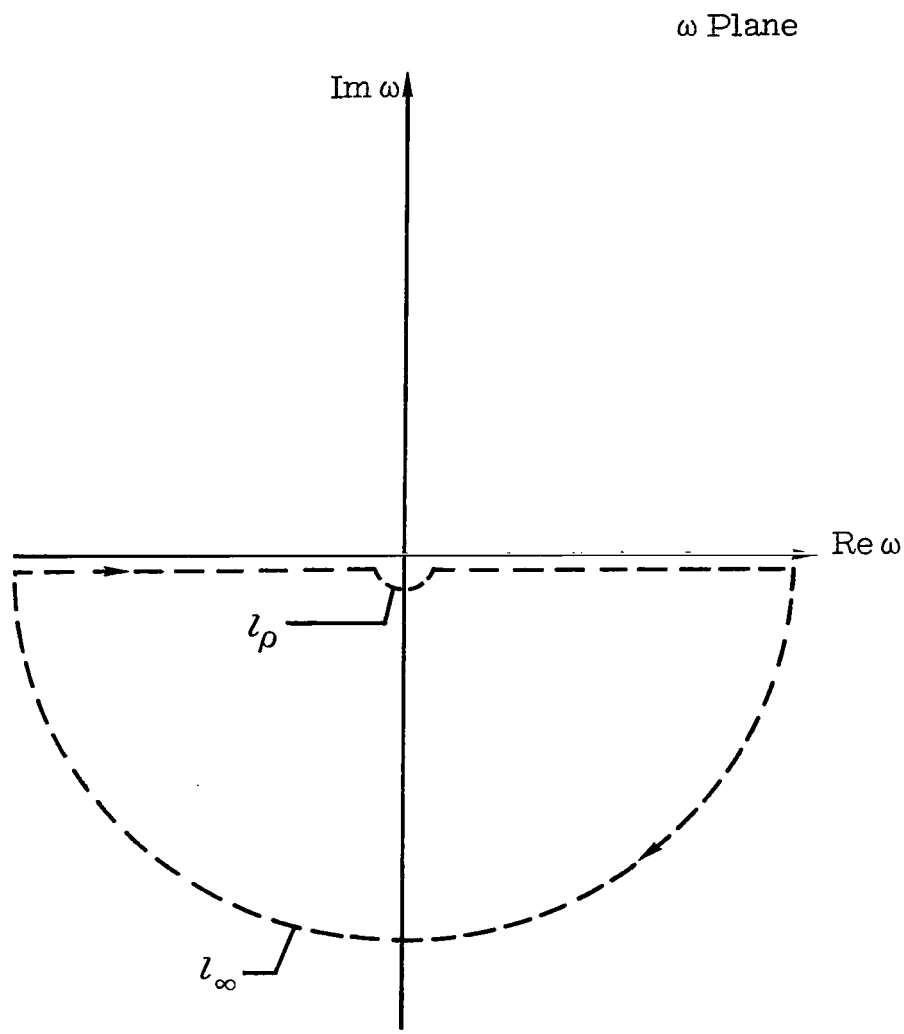

Figure 4.- Contour for evaluation of I(k).

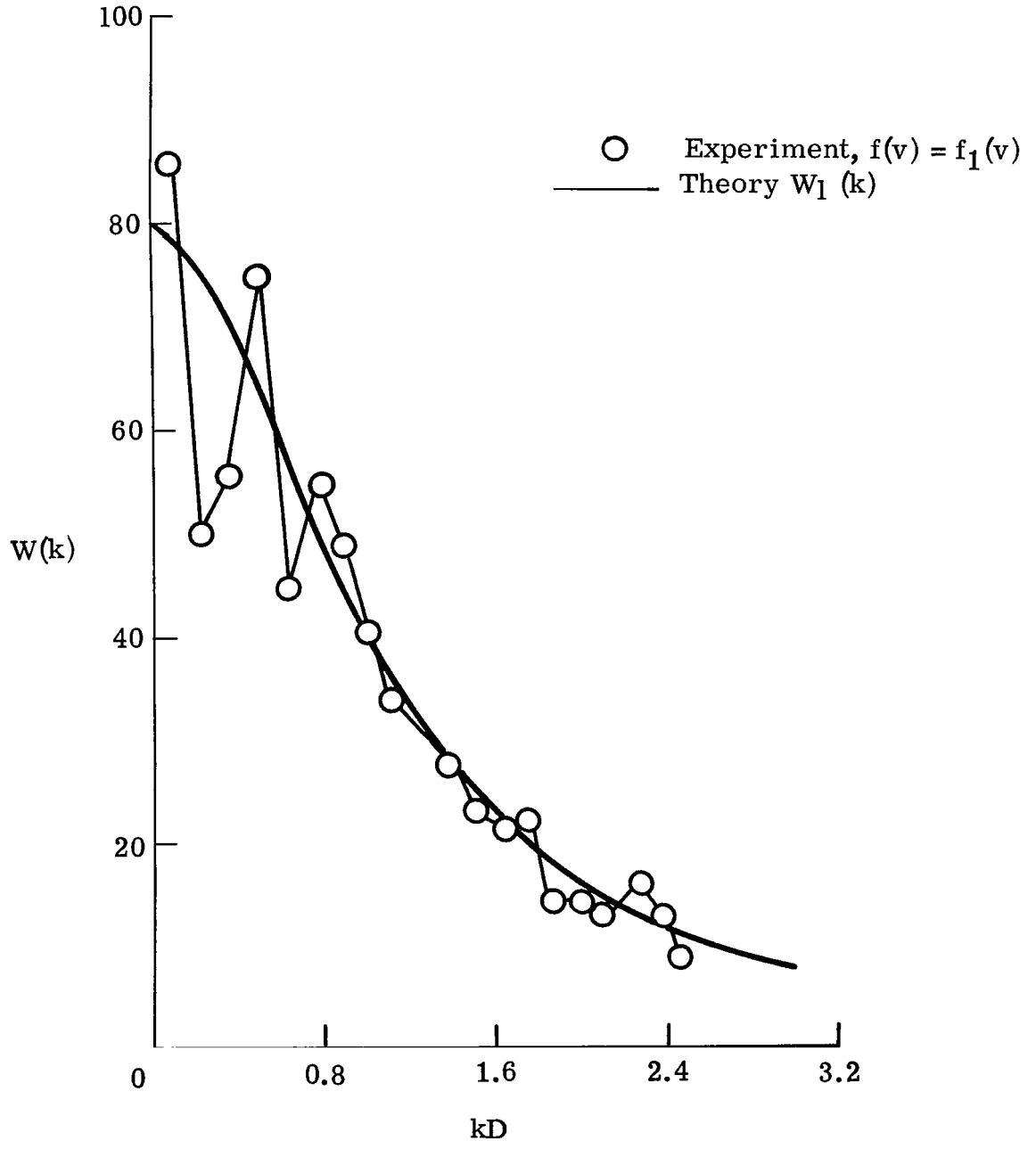

Figure 5.- Potential energy spectrum for $f(v) = f_1(v)$. N = 1000; nD = 20; Time averaged from 75 - $135\omega_p^{-1}$.

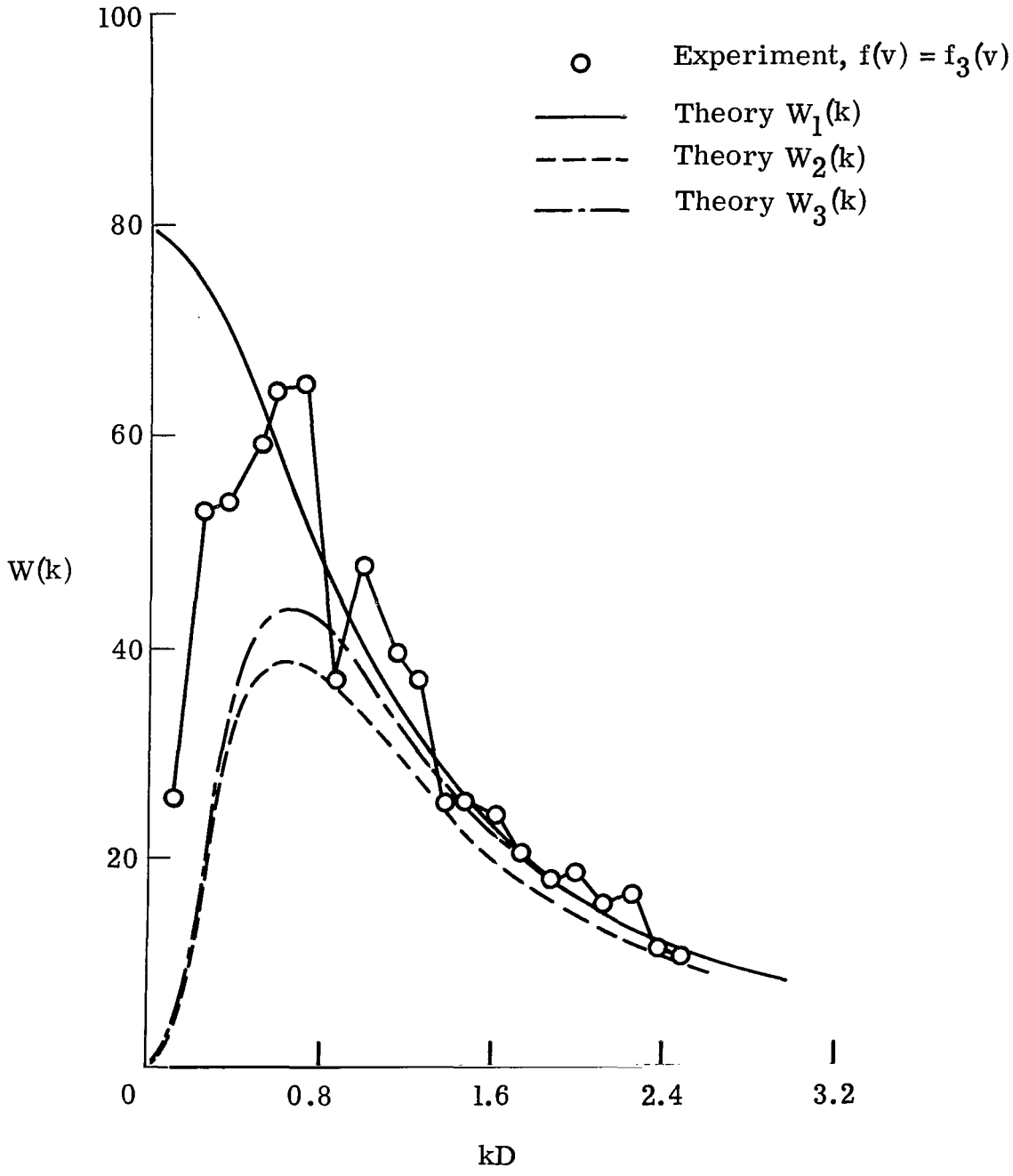

Figure 6.- Potential energy spectrum for $f(v) = f_3(v)$. N = 1000; nD = 20; Time averaged from 75 - $135\omega_p^{-1}$.

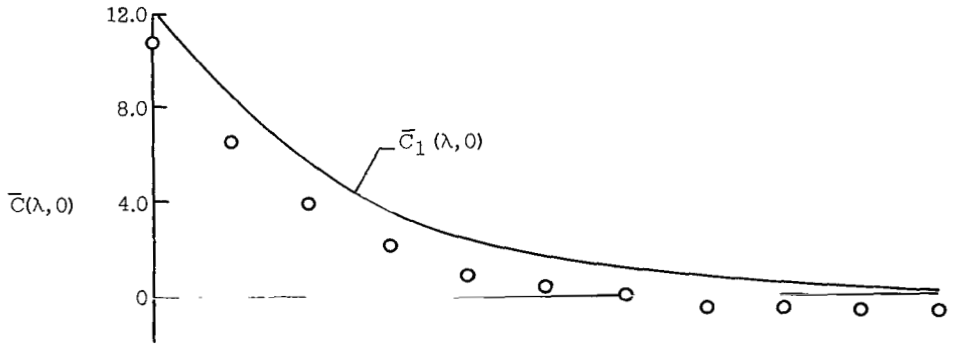

(a) $T = 40\ \omega_p^{-1}$.

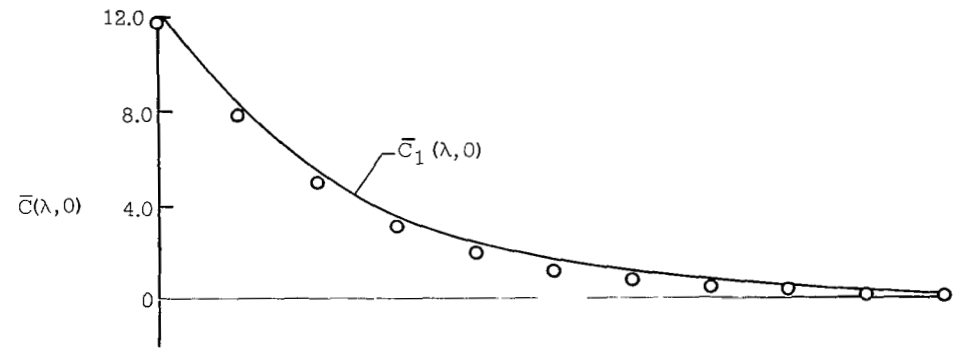

(b) $T = 100\ \omega_p^{-1}$.

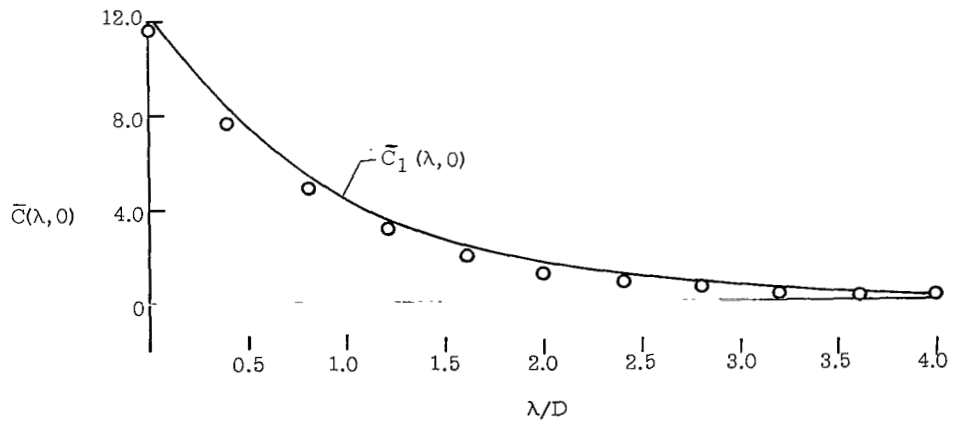

(c) Average, $T = 60 - 240\ \omega_p^{-1}$.

Figure 7.- Electric field correlation $\bar{C}(\lambda)$ for $f(v) = f_1(v)$.

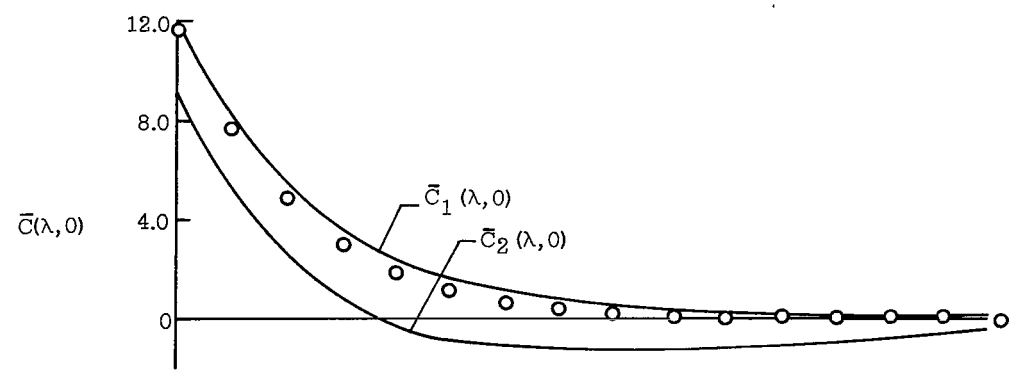

(a) $T = 40\ \omega_p^{-1}$.

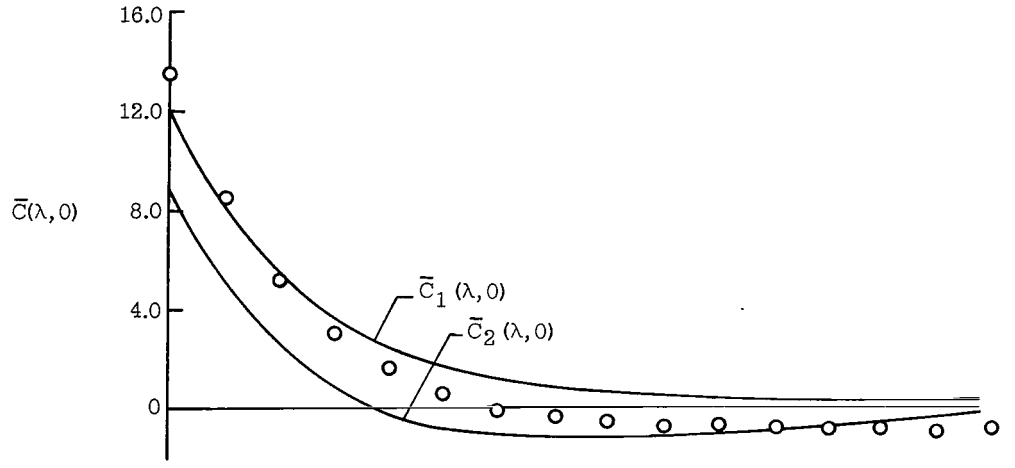

(b) $T = 100\ \omega_p^{-1}$.

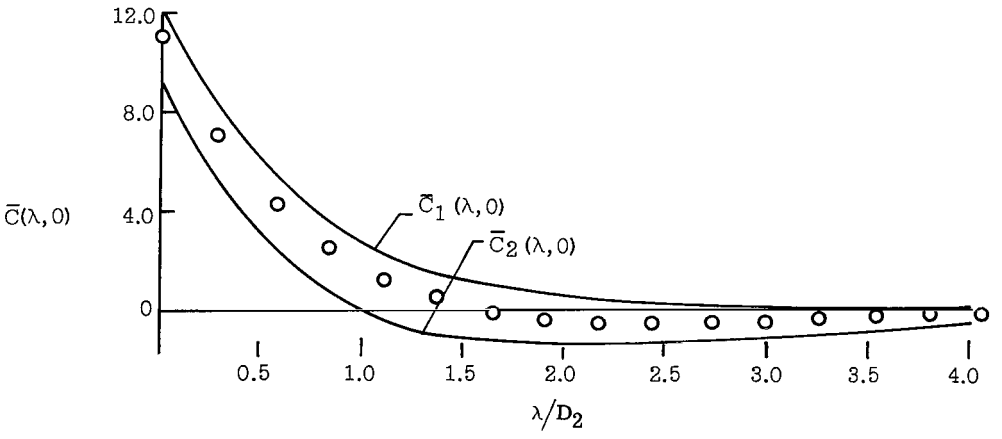

(c) Average, $T = 60 - 300\ \omega_p^{-1}$.

Figure 8.- Electric field correlation $\bar{C}(\lambda)$ for $f(v) = f_3(v)$.

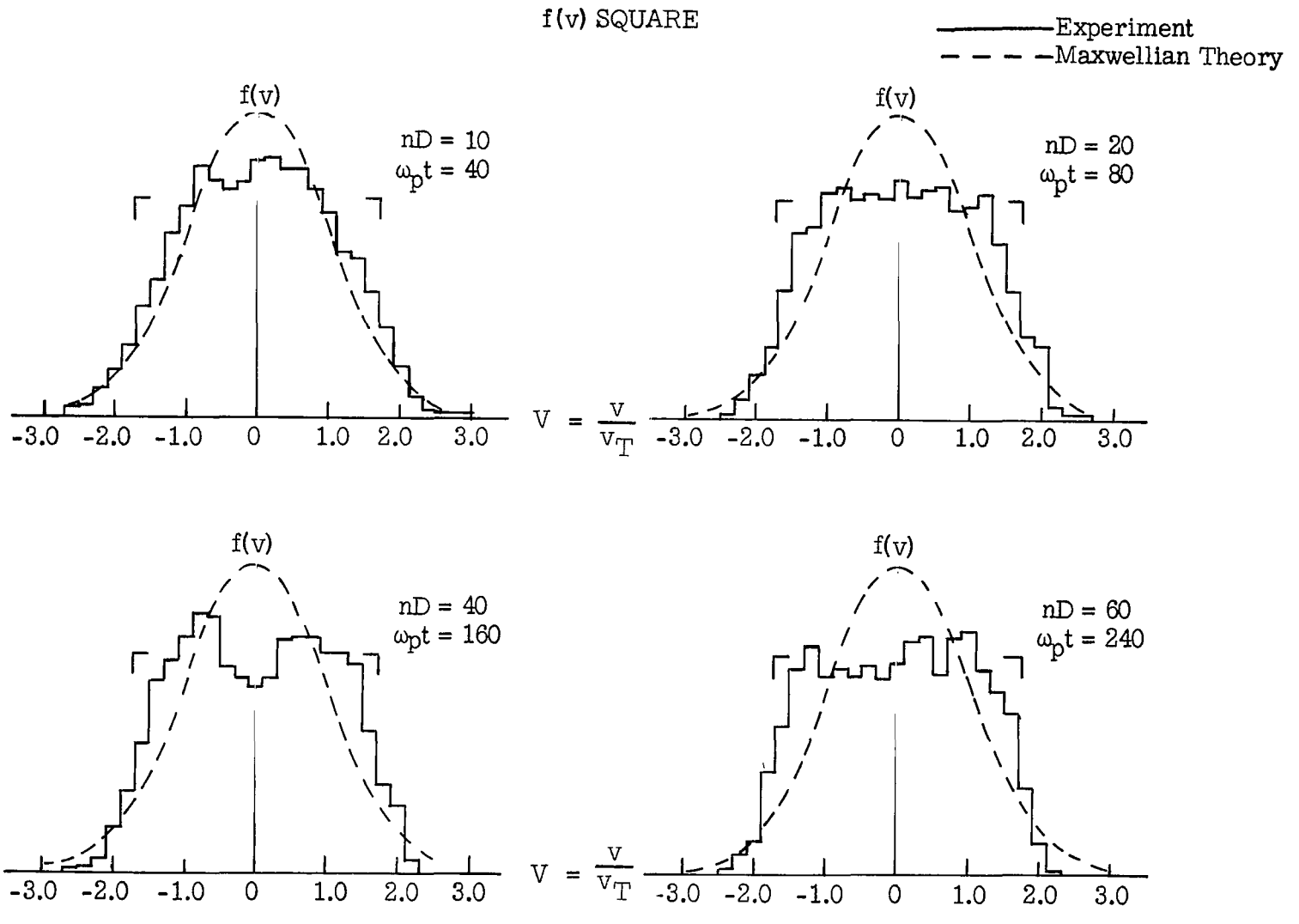

Figure 9.- Velocity distribution metaequilibrium.

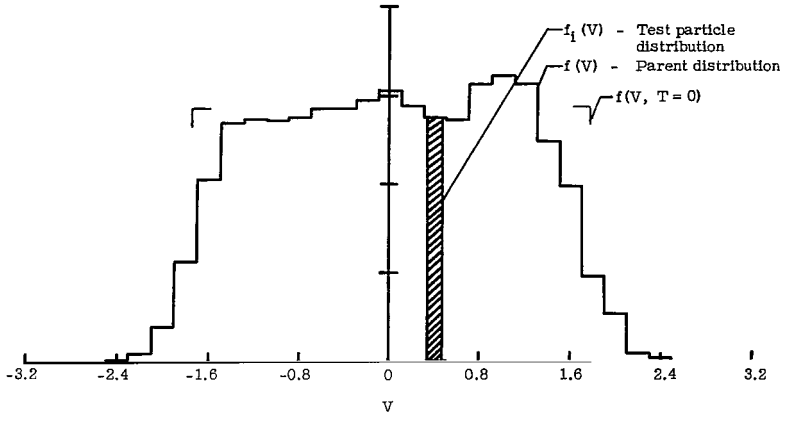

(a) $f_i(V)$ at $T = T_0$. $T_0 = 30\omega_p^{-1}$; $\langle V_i \rangle = 0.4$.

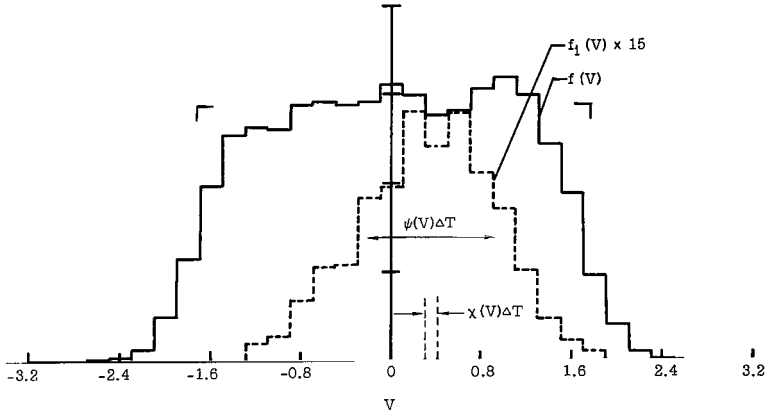

(b) $f_i(V)$ at $T > T_0$. $T = 42\omega_p^{-1}$; $\langle V_i \rangle = 0.3$.

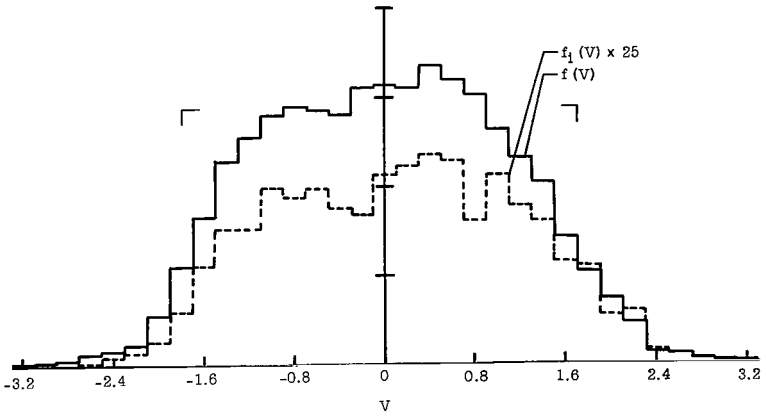

(c) $f_i(V)$ at $T_0 < T < T_0 + \frac{(nD)^2}{\omega_p^2}$. $T_0 = 230\omega_p^{-1}$; $\langle V_i \rangle = 0.1$.

Figure 10.- Relaxation of test particles.

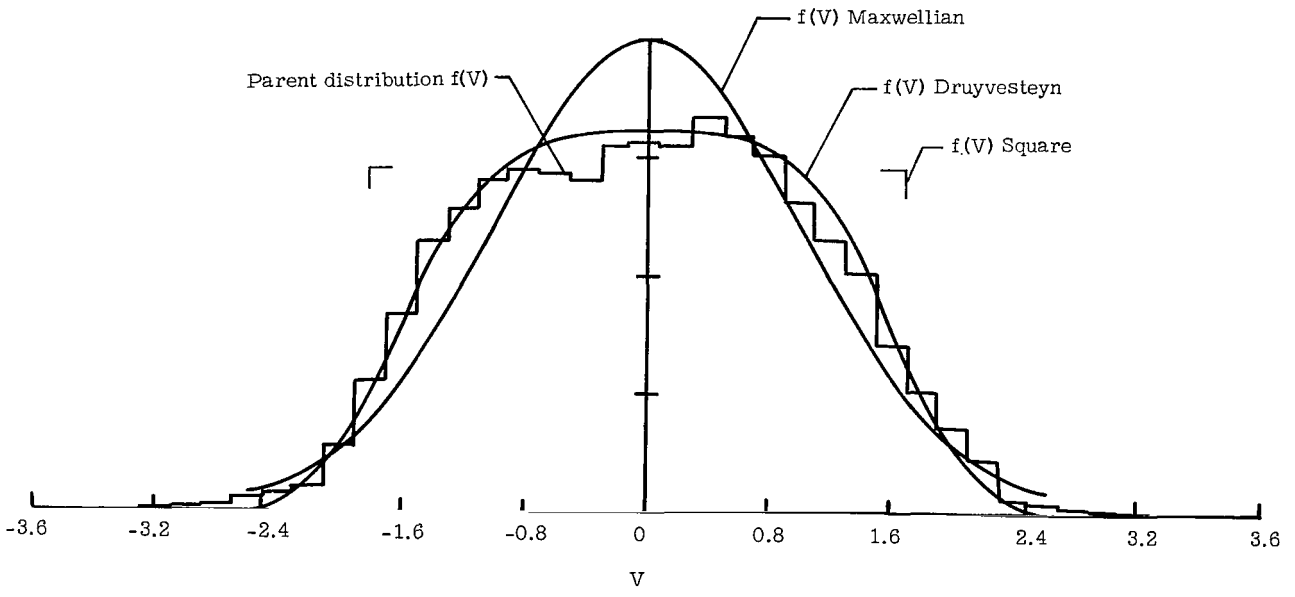

(a) Parent distribution f(V).

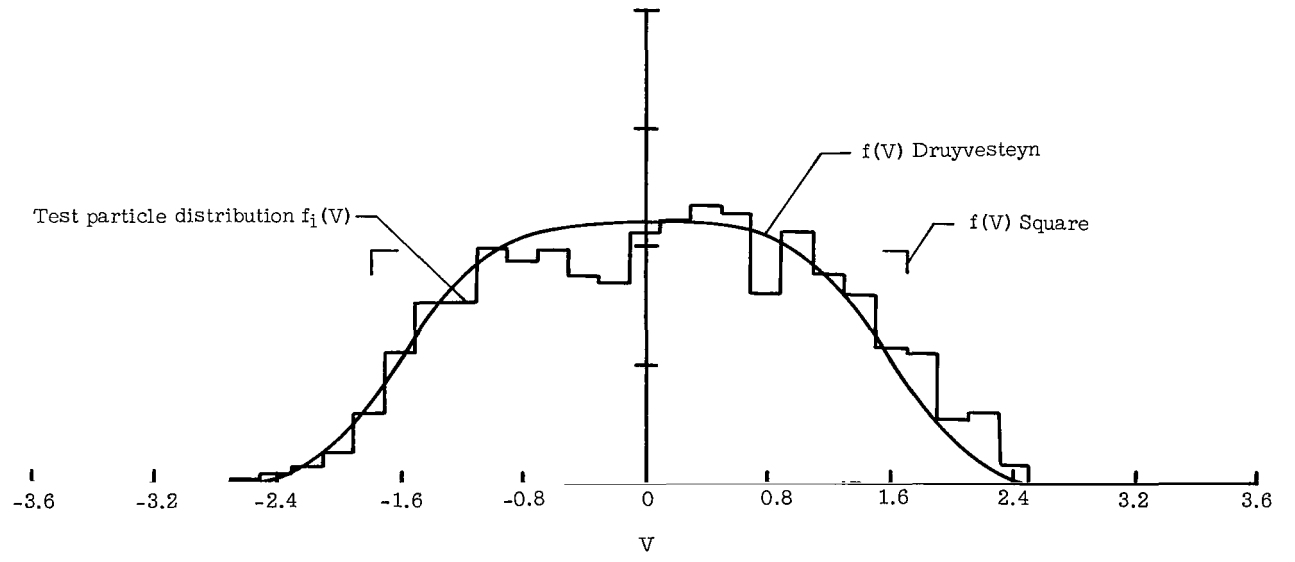

(b) Test particle distribution $f_i(V) \times 25$.

Figure 11.- Comparison of test particle and parent distributions with theory at $T = 230\omega_p^{-1}$.

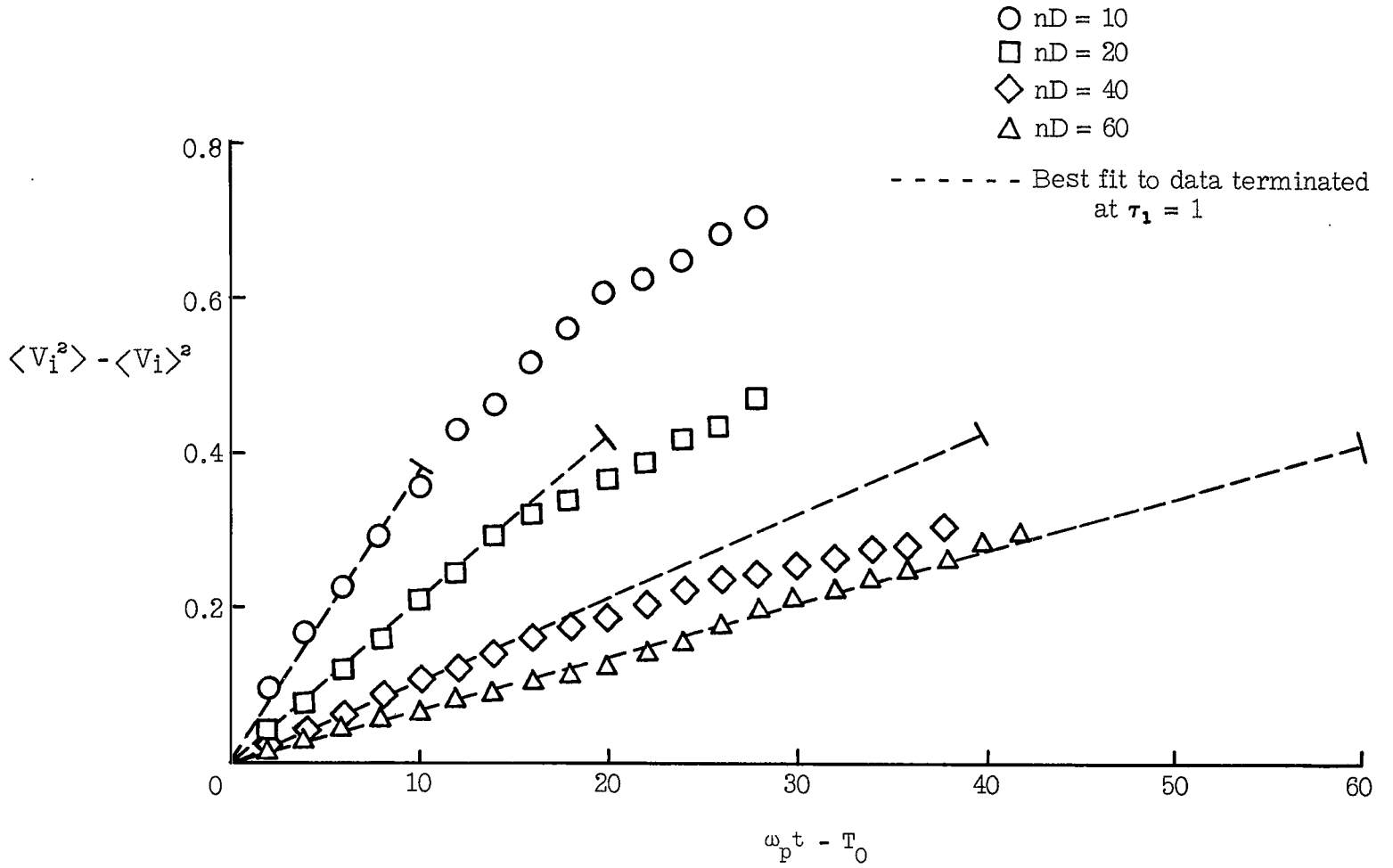

Figure 12.- Test particle diffusion for $f(v) = f_1(v)$. $T_0 = 20\omega_p^{-1}$; $(V_i)_0 = 0$.

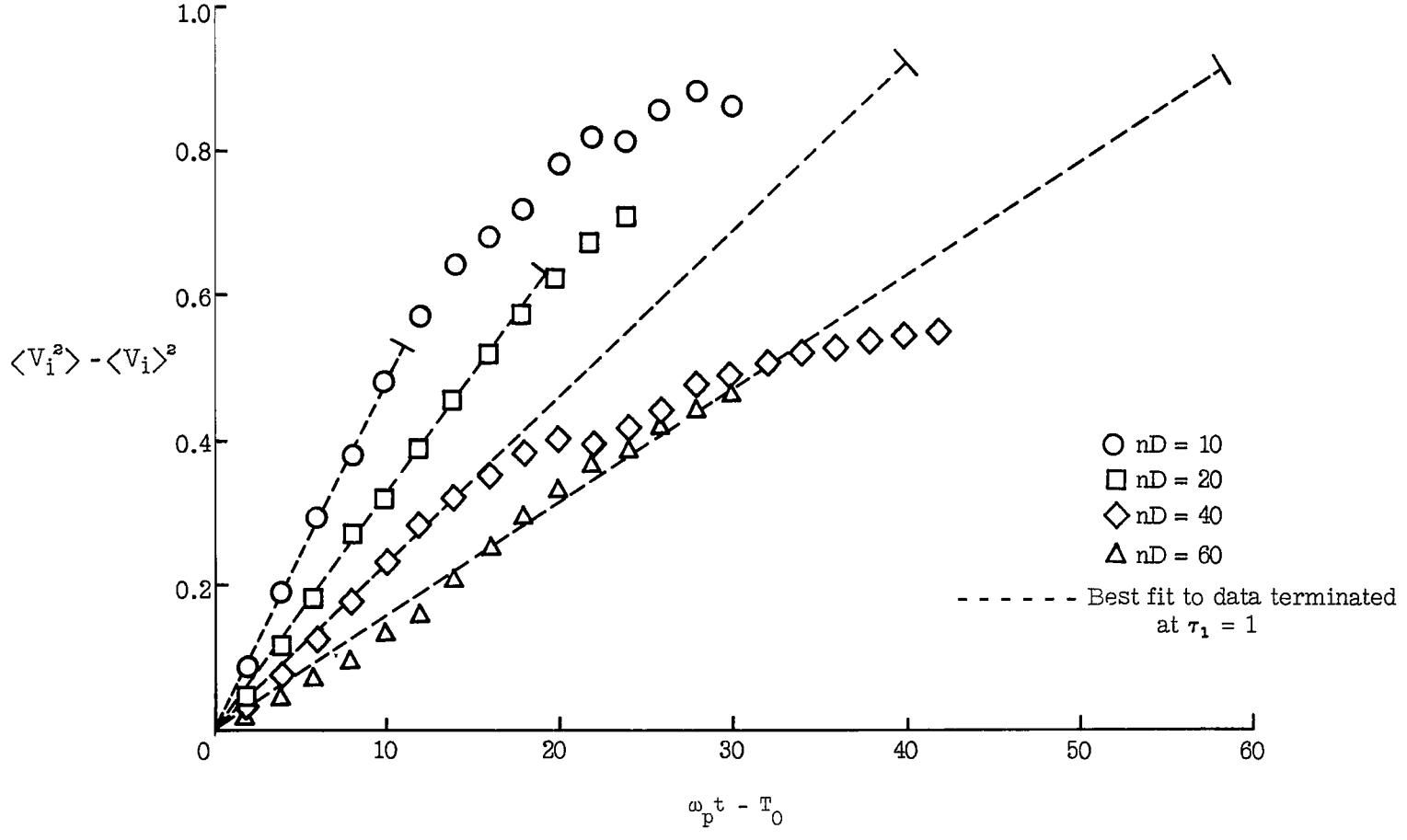

Figure 13.- Test particle diffusion for $f(v) = f_3(v)$. $T_0 = 20\omega_p^{-1}$; $(V_i)_0 = 0$.

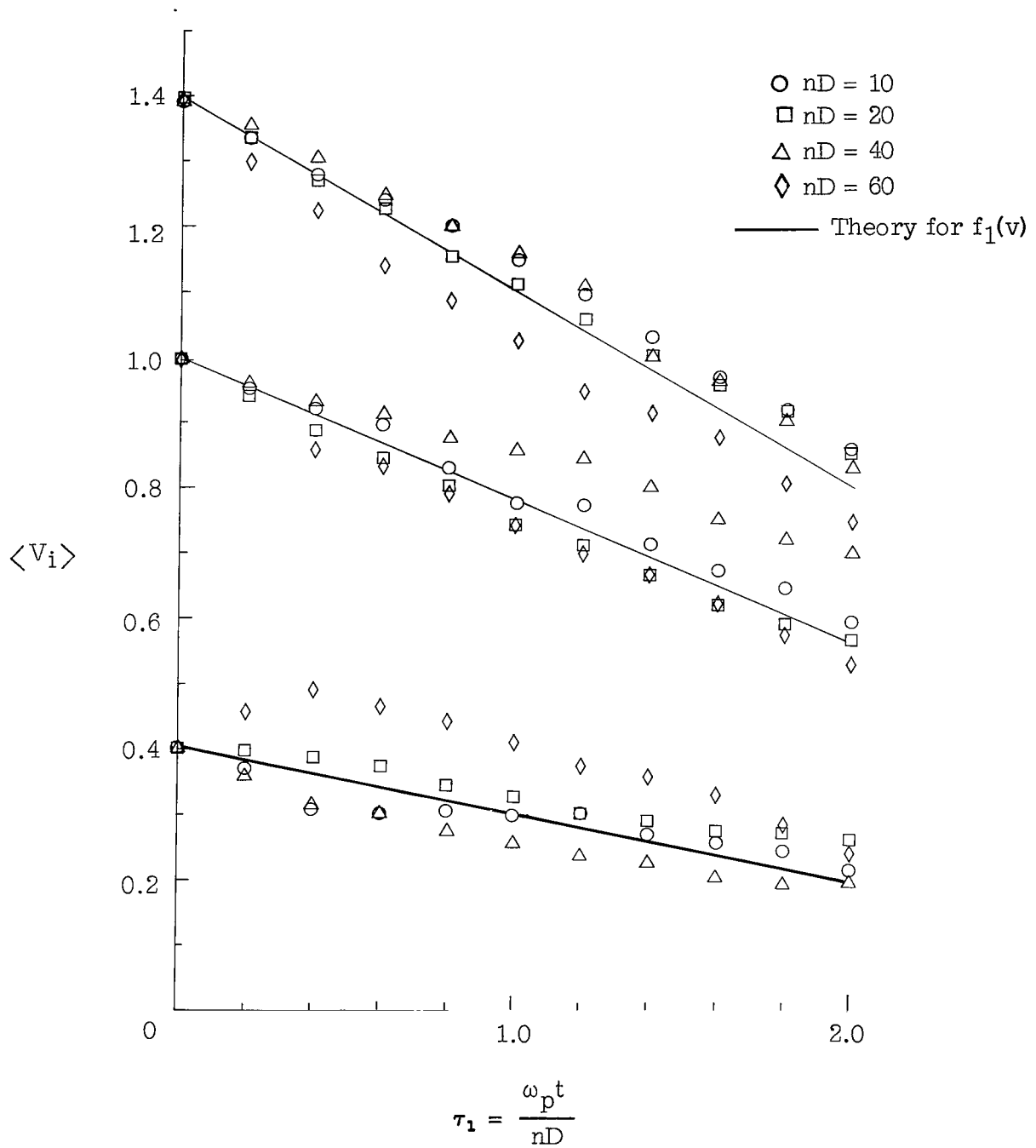

Figure 14.- Test particle drag. $f(v) = f_1(v)$. $T_0 = 20\omega_p^{-1}$.

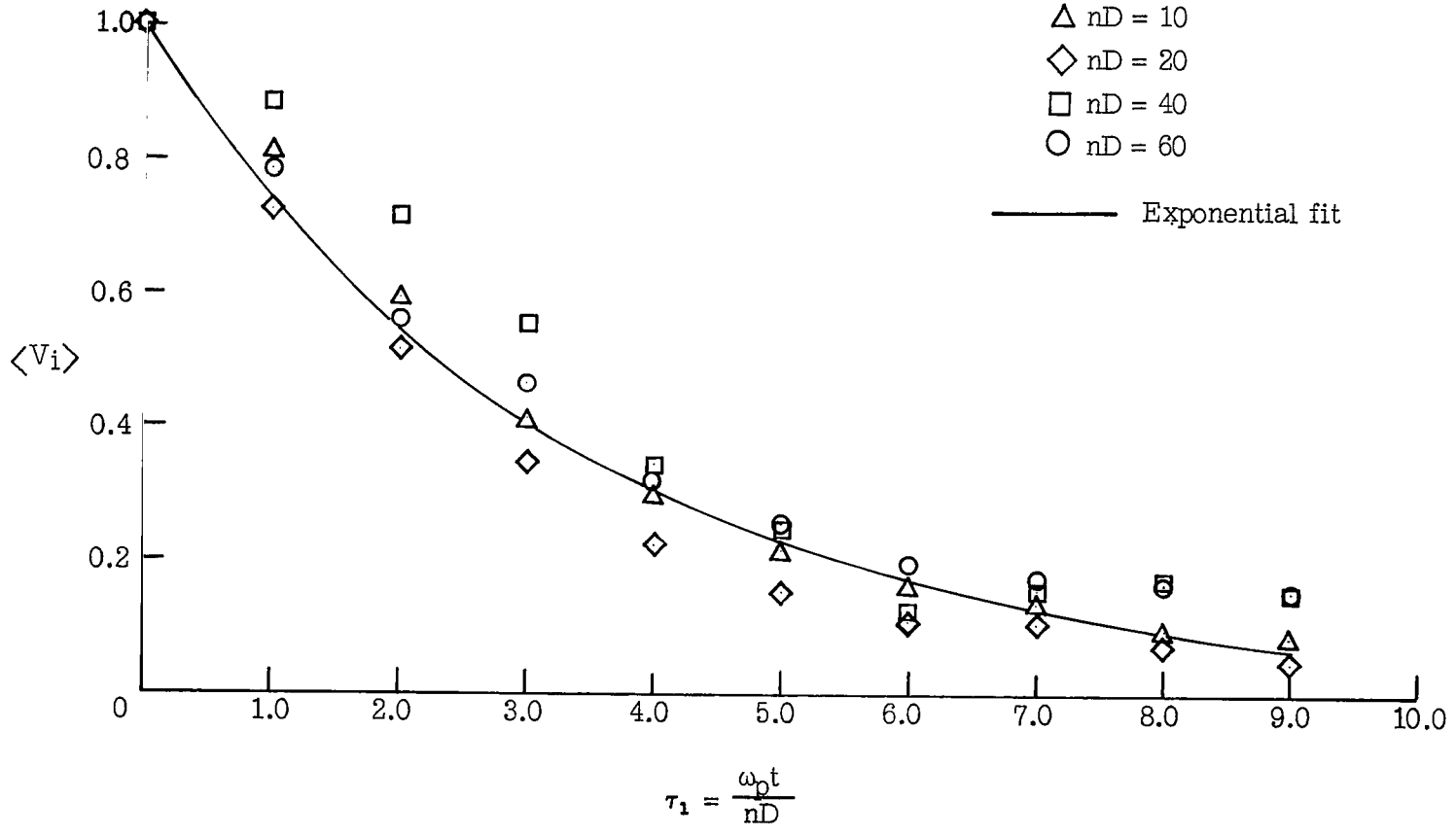

Figure 15.- Test particle relaxation. $f(v) = f_1(v)$; $T_0 = 20\omega_p^{-1}$.

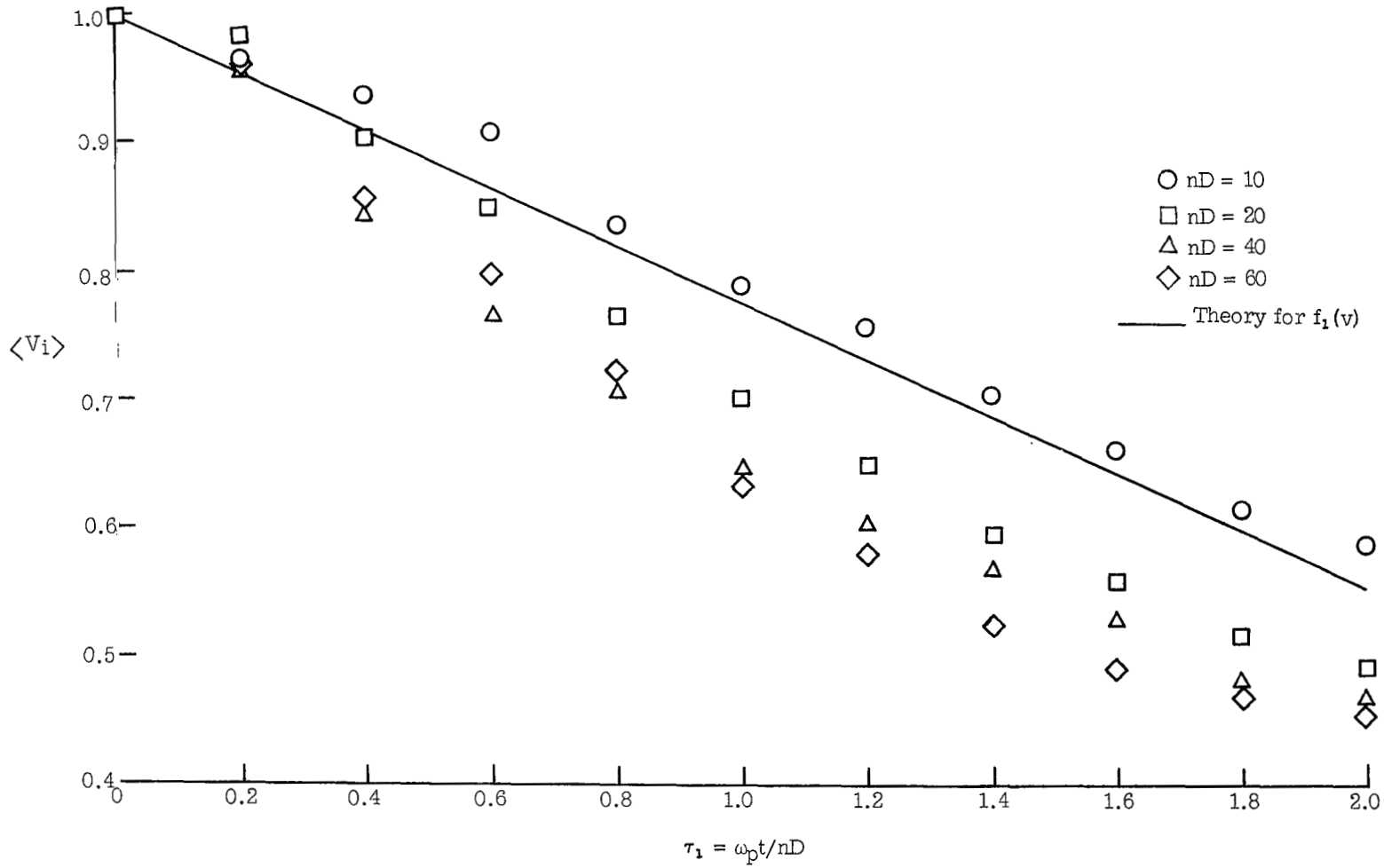

Figure 16.- Test particle drag. $f(v) = f_3(v)$; $T_0 = 20\omega_p^{-1}$.

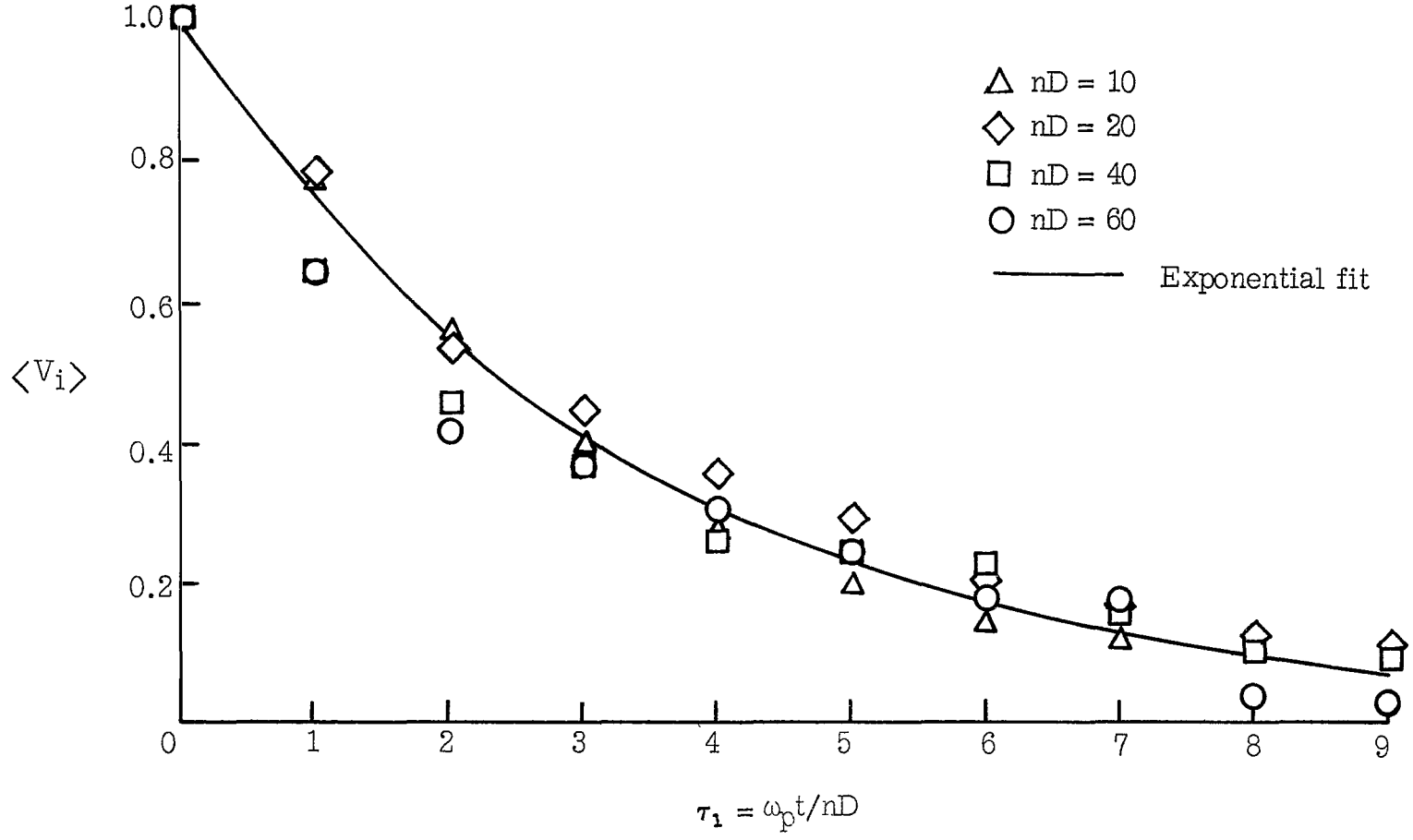

Figure 17.- Test particle relaxation. $f(v) = f_3(v)$; $T_0 = 20\omega_p^{-1}$.